universität wien

MASTERARBEIT / MASTER'S THESIS

Titel der Masterarbeit / Title of the Master's Thesis

First Principles Simulation of Ion Implantation Into Graphene

verfasst von / submitted by

Gudrun Pötzelberger, BSc

angestrebter akademischer Grad / in partial fulfilment of the requirements for the degree of

Master of Science (MSc)

Wien, 2021 / Vienna, 2021

Studienkennzahl lt. Studienblatt / degree programme code as it appears on the student record sheet:	A 066 876
Studienrichtung lt. Studienblatt / degree programme as it appears on the student record sheet:	Masterstudium Physik
Betreut von / Supervisor:	Ass.-Prof. Dr. Toma Susi
Mitbetreut von / Co-Supervisor:	Alexander Markevich, MSc PhD

Abstract

Incorporating heteroatoms into graphene allows the modification of its electronic and magnetic properties. One way to achieve this is by implanting dopants via ion irradiation. For 2D materials such as graphene, the energy of the ions has to be within a small energy window to allow them to be retained in the atomically thin lattice. In this thesis, the implantation of different atoms into a single layer of graphene is modelled with the use of density functional theory based molecular dynamics. The goal was to find out which initial energies allow B, C, N, Al, Si, P, Mn, Ni and Ge to be implanted at four different impact points in the lattice. The minimum and maximum implantation energies were successfully calculated for these nine elements and some systematic trends were observed. These results will help improve experimental ion implantation into graphene by giving a first estimate of how high an irradiation energy should be chosen for each ion species.

Zusammenfassung

Heteroatome in Graphen einzubinden erlaubt es, seine elektronischen und magnetischen Eigenschaften zu modifizieren. Eine mögliche Vorgangsweise ist die Implantation von Dotanden durch Ionenbestrahlung. Für 2D Materialien wie Graphen muss dabei die Energie der Ionen innerhalb eines kleinen Energiefensters liegen, um es dem atomar dünnen Gitter zu erlauben, sie zu halten. In dieser Arbeit wird die Implantation verschiedener Atome in eine Graphenschicht mittels Dichtefunktionaltheorie-basierender Molekulardynamik modelliert. Das Ziel war es, herauszufinden für welche Energien B, C, N, Al, Si, P, Mn, Ni und Ge in vier verschiedenen Einschlagspunkten implantiert werden können. Es ist gelungen, die minimale und maximale Implantationsenergien für diese neun Elemente zu finden, und einige systematische Trends zu beobachten. Diese Ergebnisse werden die experimentelle Ionenimplantation in Graphen verbessern, indem sie eine erste Einschätzung über die benötigte Energie der Ionenbestrahlung für die jeweilige Ionenart geben.

Acknowledgements

I would like to thank my supervisors Toma Susi and Alexander Markevich for all their guidance, support and advice, which was invaluable for my research and in making this document into a readable and coherent thesis.

My thanks also go to all the members of our research group, who warmly welcomed me and created such a friendly work environment.

Furthermore, I would like to thank my parents, who have always supported and encouraged me.

Contents

1 Introduction

1.1 Motivation

Graphene[1] is a two-dimensional material of sp^2-bonded carbon atoms arranged in a 2D-hexagonal lattice. It exhibits many interesting properties, such as excellent electrical[2] and thermal[3] conductivity and remarkable mechanical strength,[4] making it an ideal material for novel devices.[5]

Graphene is the strongest material ever measured with an intrinsic strength of 130 GPa[4] and a Young's modulus close to 1 TPa, demonstrating the potential of graphene in applications such as flexible electronics and ultra-strength composites.[6] Its thermal conductivity at room temperature has been measured as large as $5 \cdot 10^3$ W/(m K),[3] much larger than that of graphite, which has about $2 \cdot 10^3$ W/(m K).[7] At room temperature and lower, graphene has a negative thermal expansion coefficient (TEC) of about $-7 \cdot 10^{-6}$/K, which is a larger magnitude than for graphite, which has $-1 \cdot 10^{-6}$/K.[8] A negative TEC means that graphene contracts with rising temperatures. For annealed suspended graphene, an electron mobility of 200 000 $\mathrm{cm}^2/(\mathrm{V\,s})$ has been measured, which is among the highest electron mobilities of any material.[2]

Graphene-based electronic devices have shown promise for applications in DNA-sequencing,[11] photovoltaics,[12] and gas detection.[13] It has a very high conductivity which changes rapidly when gas molecules adsorb on its surface, making it an excellent candidate for high-sensitivity sensors.[9] However, pristine graphene is a zero-bandgap material,[14] which severely limits its potential uses in electronic devices due to the poor on-off current ratio,[1] which makes the electronic devices have low operation controllability.[10] A bandgap may be opened up by various means, such as reducing graphene's dimensions[15] (graphene nanoribbons and nanodots),[16] applying an electric field,[17] introducing defects or adatoms,[18] or incorporating heteroatoms into the material.[19]

Doping graphene with boron or nitrogen causes it to have p-type or n-type conductivity respectively. Moreover, N-doped graphene behaves as a semiconductor with a large on/off current ratio. However, it has lower carrier mobility (about $200-500$ $\mathrm{cm}^2/(\mathrm{V\,s})$) and lower conductivity than pristine graphene.[9] Doping graphene with other heteroatoms can open up different new areas of research, for example the introduction of local magnetism into the lattice by incorporating transition metal atom impurities with magnetic moments.[10]

Introducing substitutinal impurities into graphene allows for the modification of its elec-

tronic and magnetic properties,[20] making it possible to use graphene for new applications, such as graphene sheets doped with non-metallic atoms, which have been shown to be promising sustainable metal-free catalysts.[21] Graphene-based materials doped with various heteroatoms have also been suggested for applications in supercapacitors, sensing, energy conversion and storage.[22]

There are various ways of incorporating heteroatoms into graphene. There are chemical methods, which have certain disadvantages, such as poor control over dopant concentration and bonding configuration, contamination and inferred secondary impurities, instability, and site selectivity.[19] Low-energy ion irradiation is an alternative to chemical methods, and it is the subject of this thesis.

Low-energy ion irradition is a way of implanting heteroatoms[19] that has many practical advantages, such as being a clean, highly efficient method which is universally usable for most dopant species.[10] It is a highly developed technique used in semiconductor manufacturing to modify material properties, and thus ion implantation doping in graphene can be directly compatible with integrated circuit (IC) technologies.[10]

Being able to selectively implant heteroatoms into graphene would open up many possibilities, such as creating spatially non-uniform graphene-based materials where differently doped areas could be made.[19]

Although ion implantation is widely used in the semiconductor industry[23] to introduce dopants into materials, it is challenging in the case of 2D-materials. Successful implantation in a graphene layer can only occur for ions within a small range of kinetic energies, because an energy that is too high would send the ion right through the lattice, while an energy that is too low obviously does not allow the ion to eject a carbon atom in order to implant. Thus, the initial energy of the ion has to be between these two cases. As it is very work-intensive to implant ions into materials in practice, it is useful to simulate the implantation beforehand, in order to find out which energies have to be used to achieve implantation.

So far, the optimal energy has only been predicted for a few elements, and there are no systemical studies for implantation of ions in graphene. It has been predicted from molecular dynamics (MD) simulations that direct doping of B and N atoms in a graphene lattice could be achieved via low-energy ion implantation,[24] and this was later realised experimentally, with the successful doping being confirmed using high-resolution transmission electron microscopy.[19] The implantation of Si into graphene has also been simulated,[10] and the implantation of P has been demonstrated experimentally.[25] However, in most previous computational studies, theoretical modelling of ion implantation was performed using classical interatomic potentials, which lack the accuracy of the density functional theory (DFT) approach when it comes to chemical bond breaking and formation. It has also been theoretically as well as experimentally demonstrated recently that an ion as heavy as Ge can be implanted into graphene.[26] This is important information, as heavier ions are expected to be more difficult to implant than lighter atoms, due to

the fact that heavier atoms do not transfer as much of their energy in a head-on elastic collision, as will be discussed in Section 1.1.1.

Studies of heteroatoms in graphene using atomically resolved microscopy have been performed for N,[27] B,[28] P,[25] Si[29] and Ge.[30] Elements with a larger covalent radius than carbon cannot directly fit into the 2D lattice as a single carbon substitution, and tend to form stable structures by protruding outside the graphene plane, or by substituting for two carbon atoms.

1.1.1 Goals and Approach

For the process of ion implantation, a positively or negatively charged ion is accelerated to a certain kinetic energy to collide with the material it is to be implanted in, so that it knocks out at least one C atom and takes its place in the lattice (substitution). In this work, this process is simulated by giving the atom that is to be implanted a certain initial energy to move towards the graphene in a perpendicular direction. To reduce the complexity of the simulations, the atom that is implanted is not simulated as positively or negatively charged, and thus, it is not actually simulated as an ion. However, it has been shown that for small charges, this does not make a difference,[31] since graphene effectively neutralizes incoming charged particles.[32] The atom that is being shot at graphene will nevertheless be called an ion in this work, for the purpose of linguistic clarity when comparing these simulations and experimental studies.

Graphene is a single layer of atoms, therefore there is just a small energy window for implantation: if the initial energy of the ion is too low, the ion is reflected by the graphene layer or becomes an adatom, but if the energy is too high, the ion is transmitted through the graphene layer. Only for an initial energy between these two cases does the ion implant into the lattice. This work's purpose is to predict the initial energy that different ions need to implant into the lattice. For this, four impact points have been considered:

(a) head-on impact on the C atom ('head-on', Figure 1.1a);

(b) impact in the center of the bond between two carbon atoms ('bond-center', Figure 1.1b);

(c) impact in the center of a graphene-hexagon ('hexagon-center', Figure 1.1c);

(d) impact between the center of the hexagon and the head-on impact point, so that not only high-symmetry points are included ('asymmetric', Figure 1.1d).

Nine elements have been examined: B, C, N, Al, Si, P, Mn, Ni, and Ge. B and N are natural choices of dopants for graphene, having one electron less and more than C, respectively. They are also of a similar size to carbon, so they can be effectively incorporated into the lattice with almost no distortions of the surrounding lattice. Al, Si and P are have the same number of electrons in their outer shell as B, C and N. These elements as well as Ge were chosen to see whether the mass and radius of the ion

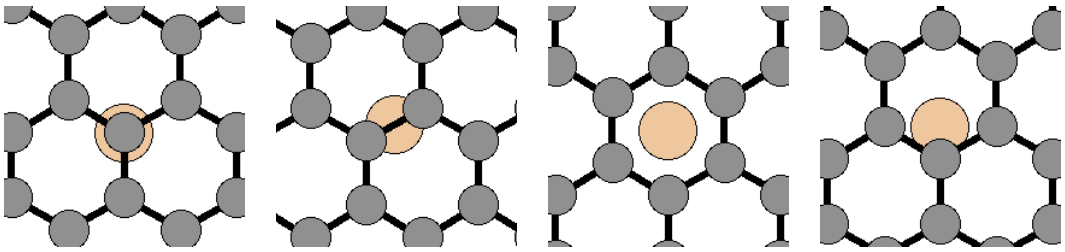

(a) head-on. (b) bond-center. (c) hexagon-center. (d) asymmetric.

Figure 1.1: The four impact points for the ion in the graphene lattice.

makes a significant difference to implantation. Mn and Ni were chosen as ions because they are transition metals, which are interesting impurity atoms to take a closer look at as they can introduce magnetism[33,34] and significantly improve the catalytic abilities of graphene.[21,35]

For each of these elements, multiple simulations have been done for each of the four impact points shown in Figure 1.1. The minimum as well as the maximum implantation energy for each case has been found using an approach similar to the bisection method. For example, to find the minimum implantation energy, the first step is the calculation of the trajectory of the ion colliding with graphene at a certain point and with a certain initial kinetic energy. This trajectory is analyzed to verify if the ion implants, is transmitted, or does not penetrate the lattice. The next calculation is started with the ion having its initial energy in the middle between the energy it had in a trajectory where the ion implanted and the energy it had in a trajectory where the ion didn't penetrate the lattice. This process is repeated until the energy is found which does allow implantation, and for which the energy that is 1 eV smaller does not allow implantation. The maximum implantation energy is found in an analogous way.

For the impact point in the center of the hexagon, implantation is not possible, as no C atom is ejected. For this case, only one energy is found, namely the minimum initial energy the ion needs to have in order to be transmitted through the lattice E_{trans} (transmission threshold).

Elastic Energy Transfer

The equation for head-on elastic collision energy transfer was derived from energy and momentum conservation laws. The result is:

$$E_{2,f} = \frac{4m_2m_1E_{1,i}}{(m_1+m_2)^2} \tag{1.1}$$

where $E_{2,f}$ is the final energy of the atom that is being hit, and $E_{1,i}$ is the initial energy of the atom that is doing the hitting. The hit atom is initially not moving, so $E_{2,i} = 0$.

Figure 1.2 shows the proportion of kinetic energy that is transferred to a carbon atom by ions with different atomic mass during the head-on elastic collision.

As Figure 1.2 shows, heavier elements transfer a smaller portion of their energy to the C atom in a head-on elastic collision. 100% of the energy is transferred if the incoming atom has the same mass as the C atom.

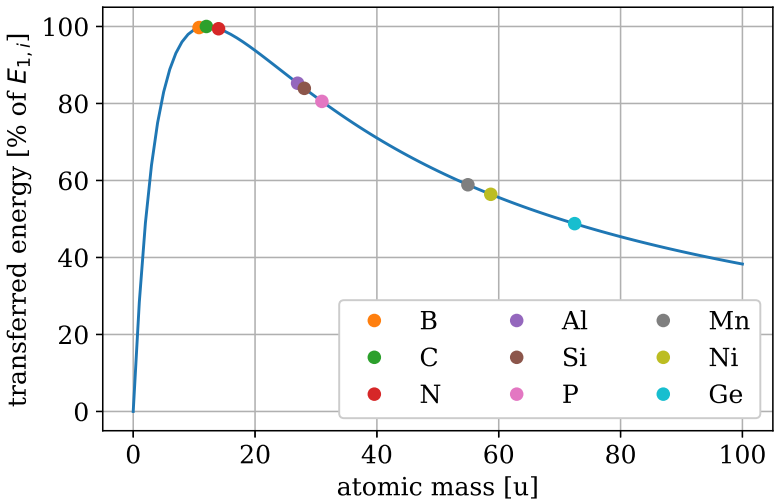

Figure 1.2: Proportion of energy that is transferred from different ions to a C atom in a head-on elastic collision, depending on the mass of the incoming ion, according to Eq. 1.1.

1.2 Theoretical Background

1.2.1 Density Functional Theory

All properties of a quantum system can be known by solving the system's Schrödinger equation. However, in practice, solving the Schrödinger equation exactly is not feasible for most systems, and so, approximations have to be made. In Density Functional Theory (DFT), all properties of the system are determined from just the electron density, instead of the many-electron wavefunction. Functionals of the electron density are used to model the quantum-mechanical ground state of the many-electron systems, so that all ground-state properties can be calculated without having to solve the Schrödinger equation of the many-electron system exactly. This substantially reduces the required computational resources and makes it possible to model systems with more electrons than would otherwise be feasible. The wavefunction of an N-electron system depends on $3N$ spacial variables (3 coordinates for each of the N electrons) whereas the density is a function of only three spacial variables.[36]

The modern DFT approach is based on the Hohenberg-Kohn theorem.[37,38]

Theorem 1. *The ground-state wavefunction of a nondegenerate electronic state is a unique functional of its electron density.*

Theorem 2. *Only the true ground-state electron density leads to the lowest energy, allowing the ground-state energy to be approximated.*

From Hohenberg-Kohn Theorem 1 it follows that there is a one-to-one mapping between the ground-state wave function and the ground-state electron density,[39] and that all ground-state properties are uniquely determined by the electron density.[36] In this way, the Schrödinger equation can be solved by finding a function of three spatial variables, namely the electron density $\rho(\vec{r})$, instead of the wavefunction that depends on $3N$ spacial variables.[39] However, Hohenberg-Kohn Theorem 1 says nothing about the form of the functional of the electron density. Hohenberg-Kohn Theorem 2 allows the functional to be approximated with the variational principle, to find the electron density associated with the lowest energy, i.e. the ground state of the system.[39] Thus, the problem of solving the many-body Schrödinger equation exactly is bypassed, replaced with the minimization of a density functional.[36]

In the practical application of DFT, a reference system (**Kohn-Sham system**) with the same ground-state electron density as the original system is defined. The electrons of the reference system are independent particles that do not interact with each other. Thus, the many-body problem of interacting electrons in a static potential is reduced to the problem of non-interacting electrons moving in an effective potential $V_{eff} = V_{ext} + V_{XC}$, where V_{ext} is the sum of the attractive potential exerted on the electrons due to the nuclei (V_{Ne}) and the classical Coulomb potential due to electron-electron interaction (V_C), and V_{XC} is the exchange-correlation potential generated by the exchange-correlation energy. Instead of interacting with each other, the particles interact with the effective potential V_{eff} that is implemented in such a way that the electron density of the reference system is the same as that of the original system. The total energy of the system is a functional of only the electron density, therefore the total energy calculated from the reference system will be the same as the total energy of the actual system, as the two systems have the same electron density. Methods for calculating the kinetic energy for the interacting system have proven too inaccurate for most purposes, therefore the kinetic energy of the non-interacting reference system is calculated instead. Since the kinetic energy of the non-interacting reference system (T_S) is not exactly equal to the kinetic energy of the interacting system (T), this is corrected for within the exchange-correlation energy.

In DFT, the energy of the (original, interacting) system is calculated as follows:

$$E(\rho(\vec{r})) = T_S(\rho) + E_{Ne}(\rho) + J(\rho) + E_{XC}(\rho) \tag{1.2}$$

where T_S is the kinetic energy of the non-interacting system, E_{Ne} is the electrons-nuclei interaction energy, J is the classical electron-electron repulsion energy, and E_{XC} is the

the exchange-correlation energy. The exchange-correlation functional $E_{XC}(\rho)$ consists of the non-classical electron-electron repulsion (self-interaction correction, exchange and correlation) as well as of the difference between the exact kinetic energy and the energy of the non-interacting system. It is the only component in DFT which cannot be calculated exactly.[40]

If V_{Ne}, V_C (the potential corresponding to the energy J), and V_{XC} are all explicitly known, then V_{eff} can be calculated from their sum. V_{eff} is needed to calculate the orbitals that define the non-interacting reference system with the same electron density as the original system. However, trying to find V_{eff} leads to a circle of dependencies: V_{eff} depends on the density ρ through the Coulomb-term, but to calculate ρ, V_{eff} is needed. Therefore, the Kohn-Sham equations have to be solved iteratively.[40]

There are many different approaches to obtaining an explicit approximation of E_{XC}. The local density approximation (LDA) assumes that E_{XC} is the same as it would be for homogeneous electron gas. This approximation tends to overestimate the strengths of all bonds near equilibrium, though it is exact for any uniform electron gas.[36] The generalized gradient approximation (GGA) depends not only on the electron density at each point, but also on its gradient at each point. This allows it to better describe inhomogeneous molecular densities.[36] In this work, the Perdew-Burke-Ernzerhof[41] (PBE) GGA was used, which gives accurate geometries, but tends to underestimate binding energies.

1.2.2 Description of the Wave Function

To solve the Kohn-Sham equations numerically, different methods can be used to describe the wave functions. With the finite-difference (FD) method, the wave functions are expanded on a real-space grid.[42] Another possibility is the plane-wave (PW) approach, where the wave functions are expanded in plane waves.[42] Plane waves are the solutions of the Schrödinger equation of a free particle.[40] The plane wave cutoff energy E_{cut} is the parameter that determines at which energy the basis set is truncated, so that only plane waves with an energy lower than E_{cut} are included in the basis set. For the FD mode, the precision is instead determined by the grid spacing.

In this work, instead of FD or PW, the linear combination of atomic orbitals (LCAO) expansion[43] of molecular orbitals is used to describe the wavefunctions. In the LCAO-expansion, the Kohn-Sham orbitals are linearly expanded with the help of L predefined atomic-orbital-like basis functions to increase numerical performance while in most cases retaining accurate geometries and forces.[40]

1.2.3 Description of Core Electrons

Near the nucleus, the wavefunction oscillates rapidly and is therefore difficult to compute requiring a high computational cost.[44] One solution to this problem is to use a pseudopotential[45] to describe the Pauli repulsion of the core electrons.[44] This is possible

because the core electrons' contribution to chemical bonding is negligible (frozen-core approximation).[46] The pseudo wavefunction merges with the actual wavefunction above a chosen distance from the core (cutoff-radius r_C).

However, pseudopotentials also come with disadvantages, such as the loss of information about charge density and wave functions near the core,[44] or the fact that the cutoff-radius is often specifically chosen for a system such that the results are in good agreement with experiments, or such that they are in good agreement with all-electron calculations. This leads to transferability problems, meaning the pseudopotential might only give accurate results in systems that are chemically similar to the one it was tailored to.[47]

An alternative to pseudopotentials is the augmented plane-wave approach (APW),[48] an all-electron method. Within non-overlapping spheres around the positions of the nuclei, the potential is approximated as spherically symmetric. In these atomic regions, the basis functions are composed of atom-like partial waves. In the interstitial regions in between these spheres, the potential is approximated as constant. At the interface between the atomic and interstitial regions, continuity is enforced.[44]

In this work, the projector augmented wave method (PAW)[44] is used instead to describe the core electrons. It is an all-electron method that uses concepts from both APW and the pseudopotential approach. Instead of the oscillating wavefunctions near the core, this approach uses smooth wavefunctions which are easier to work with. A linear transformation can then be used to transform the smooth pseudowavefunction into the real wavefunction, so that all-electron properties can be calculated. This method is used because it is very accurate and does not lose the information about the core electrons.[49]

1.2.4 Molecular Dynamics

In this work, density functional theory is used in combination with molecular dynamics (MD). DFT is used to calculate the energy and forces at each time step. The particles are moved according to the forces by integrating Newton's equations of motion numerically. In this work this is done using the Velocity Verlet algorithm, which preserves the total energy of the system, the number of atoms, and the volume of the system (NVE microcanonical ensemble). In this way, a trajectory of all the particles in the system can be obtained. How far the atoms are moved before the forces are re-calculated depends on the chosen timestep dt. The optimal choice of timestep depends on the system.

2 Methods

The DFT calculations were performed using GPAW[50] versions 1.4.0 to 1.5.2, a Python-based code using the PAW method. In GPAW, the wave functions can be described with plane waves (PW), atom-centered basis functions (LCAO), or real-space uniform grids with multigrid methods and the finite-difference approximation (FD).[42] In this work, GPAW's localized atomic basis set (LCAO-mode[51]) was used for the main calculations. For large systems, LCAO calculations tend to be much faster than FD or PW calculations, but also less precise.[42] It is very efficient for periodic low-dimensional systems with vacuum, which is why it was chosen for this work. A double-zeta polarized (dzp) basis set was used, meaning two basis functions per valence state and a polarization function, the Perdew–Burke–Ernzerhof (PBE)[41] functional was used to approximate E_{XC}, which is an excellent approximation for carbon materials.

GPAW relies on the Python package ASE[52] ('atomic simulation environment'), which interfaces with the DFT calculations, describing the atoms, performing molecular dynamics calculations, and handling visualization, geometry optimization, and more. Its aim is to set up, steer, and analyse atomistic simulations.[53] ASE versions 3.16.2 to 3.17.0 were used.

Periodic boundary conditions were used to mimic an infinite graphene layer. The graphene was set up in the xy-plane, and consisted of 162 C atoms (9×9 unit cells). In z-direction the graphene sheet and its periodic replicas were separated by a vacuum of 40 to 100 Å, to avoid interaction between the layers and provide sufficient space for moving ions. To visualize the trajectories, ASE's graphical user interface was used.

To calculate the electronic properties, an integration over the Brillouin zone should be performed. In practice however, this would be far too computationally expensive, and so the Monkhorst-Pack[54] grid is used for **k**-point sampling of the Brillouin zone. Fermi-Dirac smearing was used for the occupation of electronic levels.

2.1 Convergence Tests

To test the computational methods, a primitive cell of graphene was simulated (Figure 2.1). Using periodic boundary conditions, this cell becomes equivalent to an infinite graphene layer. It is used in the following to test for which **k**-point mesh and which amount of grid-points the energy of the system converges, as well as to determine the lattice constant of graphene with different computational methods.

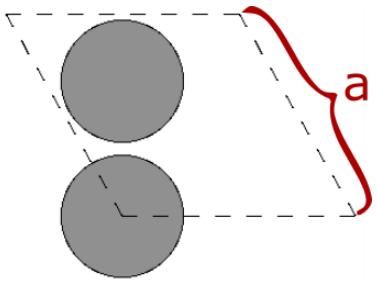

Figure 2.1: The primitive cell of graphene. The lattice constant a is marked.

2.1.1 k-points

The energy of a graphene layer was calculated for different **k**-point meshes using the cell shown in Figure 2.1, in the LCAO mode with the PBE exchange-correlation functional and the dzp basis set. The simulations used Fermi-Dirac smearing with a width of 0.01 eV, and a lattice constant of $a = 2.4817$ Å as calculated in Section 2.3. The in-plane **k**-points were varied in steps of 3. The results can be seen for a grid spacing $h = 0.1$ Å in Figure 2.2, and for $h = 0.2$ Å in Figure 2.3. As can be seen from the plots, the calculated energy depends on the chosen grid spacing, but the convergence behaviour is identical. The same calculation was done for the PW mode, for which the plot can be seen as Supplementary Figure 5.1.

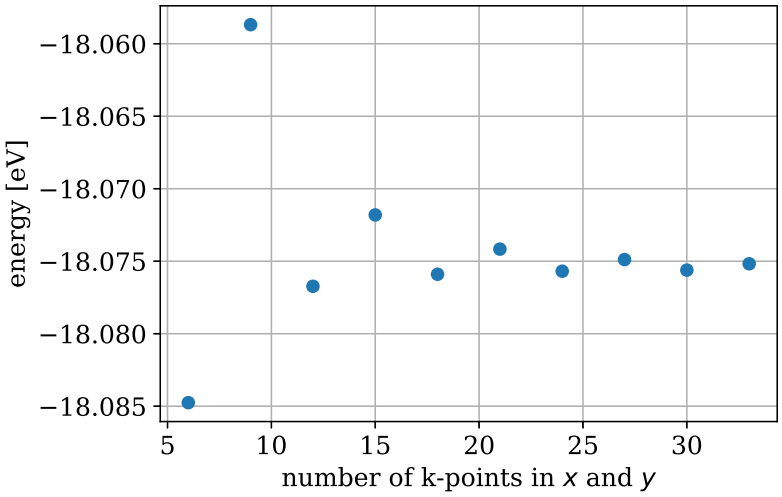

Figure 2.2: Number of **k**-points and the corresponding energy of the graphene unit cell for LCAO-mode with $h = 0.1$ Å.

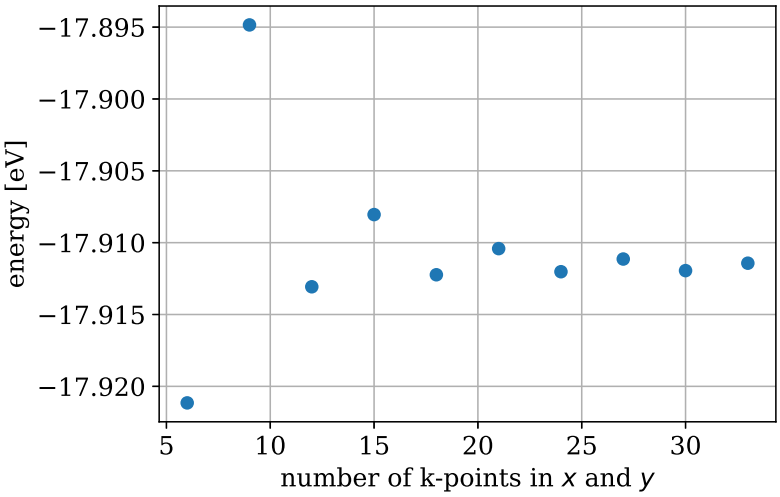

Figure 2.3: Number of **k**-points and the corresponding energy of the graphene unit cell for LCAO-mode with $h = 0.2$ Å.

2.1.2 Grid Spacing

To test which grid spacing should be used in the LCAO mode, the same system as in Section 2.1.1 was used. Grid spacing h was varied and the corresponding energies calculated, and the results are shown in Figure 2.4. A spacing of 0.2 Å provides a good compromise between accuracy and efficiency. The convergence of the PW cutoff energy can be found in Supplement 5.

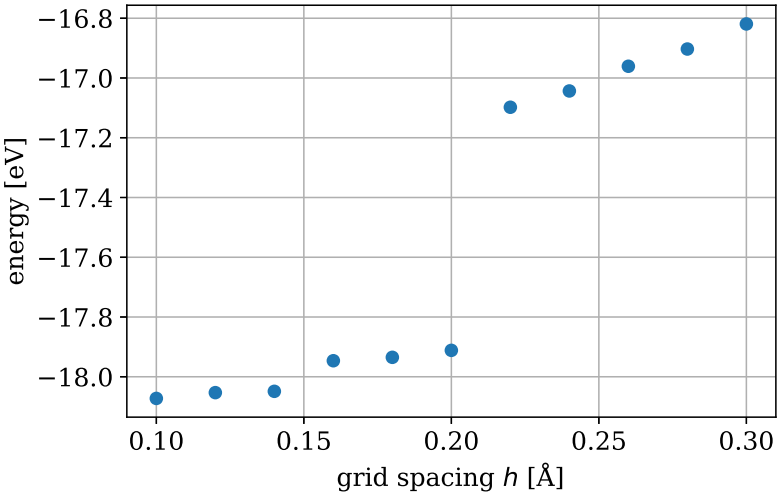

Figure 2.4: The energy of the system for different grid spacings in LCAO mode.

2.2 Atomization Energy of a C_2 Molecule

The atomization energy of a C_2 dimer was calculated and compared to literature values. This was done by first simulating a cell with just one C atom (with broken cell symmetry) and finding its potential energy E_C, and then simulating a cell with two C atoms (Figure 2.5) separated by a distance of 1.4 Å, which is close to the experimental bond-length of C_2, letting the system relax, and finding the system's potential energy E_{C2}. The atomization energy E_{atom} was calculated as

$$E_{atom} = 2 \cdot E_C - E_{C2} \tag{2.1}$$

The cell size was chosen to be $10 \times 10 \times 10$ Å so that the C atoms in periodic images do not influence each other. LCAO-mode was used with the dzp basis set and the PBE exchange-correlation potential. Fermi-Dirac smearing was used with a width of 0.01 eV. The BFGS optimization algorithm was used for optimization of the molecule.

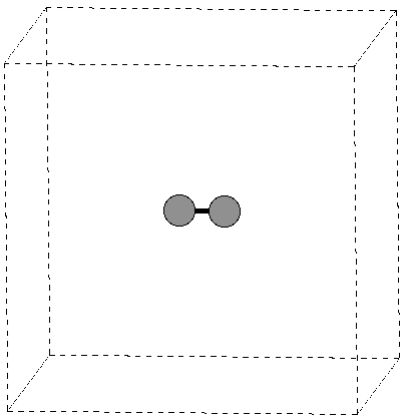

Figure 2.5: The system that was used to estimate the C_2 dimer atomization energy.

The result of the calculation is an atomization energy of 6.20 eV, and a bond length of 1.287 Å. In the computational chemistry comparison and benchmark database, the experimental bond length of C_2 is given as 1.243 Å, and the calculated one as 1.261 Å.[56]

The bond dissociation energy of C_2 according to the Active Thermochemical Tables is given by Ruscic et. al.[57] as 602.52 kJ/mol, which converts to 6.24 eV/bond, very close to the result that was obtained here.

2.3 Finding the Lattice Constant of Graphene

The lattice constant of graphene was calculated using different methods, and compared to its value in existing literature. To this end, the PBE exchange-correlation functional was used, with a **k**-point mesh of $24 \times 24 \times 1$ and Fermi-Dirac smearing with a width of 0.01 eV. For LCAO mode, the dzp basis set was used, for PW mode, a cutoff energy of 500 eV. For each mode, the equilibrium lattice constant was estimated by calculating the energy for different possible lattice constants and finding the minimum. The lattice constant in the z-direction (the distance between the graphene layers) was held constant at 20 Å. The lattice constant a for the 2D hexagonal lattice was varied between 2.45–2.58 Å. When finding the lattice constant using ASE GUI, the volume of the relaxed cell is given. To calculate the lattice constant, the following formula was derived: the lattice constant of a graphene cell can be calculated from the volume (given by ASE GUI) as:

$$a = \sqrt{\frac{V}{d \cdot \cos(30°)}}\ , \tag{2.2}$$

where a is the lattice constant (see Figure 2.1), V is the volume, and d is the height of the cell.

In PW mode, the Stress Tensor (ST) can be directly calculated, which allows automatic optimisation of the unit cell and finding the equilibrium lattice constant. Table 2.1 shows the results for the lattice constant a for the different simulations.

Table 2.1: Lattice constant of graphene [Å] calculated with different methods. h is the real-space grid spacing [Å].

	LCAO	PW	FD	ST
$h = 0.1$	2.4817			
$h = 0.18$	2.4752			
$h = 0.2$	2.4746		2.4656	
PWcutoff = 500 eV		2.4680		2.4664

The literature value for the lattice constant of graphite is 2.462 Å,[55] so if we can assume that the lattice constant for graphite is the same as that of graphene, LCAO seems to overestimate the value somewhat, while both PW and FD values are more accurate.

2.4 Energy Conservation in a Collision of Two Atoms

In order to check whether the simulations behave in a physically realistic way, energy conservation is tested for different timesteps dt, because the timestep has a significant influence on the simulations. For one thing, changing the timestep has a large effect on the amount of computing time that is needed to perform a simulation, so it is critical to set the timestep to be as big as possible in order to be able to do a fair amount of calculations in a given time and with a given amount of computing resources. On the other hand, setting a too large timestep causes the simulation to yield unphysical results. Therefore, before the main experiment is done, a suitable timestep should be chosen. For this reason, test simulations are performed for different timesteps, to see how big of a step can be chosen while still gaining accurate results in the simulations.

Specifically, two C atoms are made to collide repeatedly while the change in energies is observed. For this test, a cell with dimensions $10 \times 10 \times 10$ Å with two atoms in it is used. Giving the first atom an initial kinetic energy in the z-direction, it collides with the second atom, and due to periodic boundary conditions, the collision is repeated in a periodically replicated cell. By letting this collision happen many times, energy conservation can be verified, as small changes in energy will add up, and it will become clear if the energy diverges over time. If the peaks in kinetic energy line up, then the collisions are elastic, as is expected. Peaks which are not aligned suggest that the timestep was too large. This allows the selection a timestep which is as large as possible to have minimal computational cost, but small enough to yield physically realistic results. In this way, a value for the timestep can be chosen that is a compromise between accuracy and computational cost.

Unless specified otherwise, all simulations were done using the LCAO method, the PBE-functional and dzp basis set, with a density convergence criterion of 10^{-5}, a **k**-points mesh of $1 \times 1 \times 1$, and grid points gpts $= (48 \times 48 \times 48)$, leading to a grid spacing of $h = 0.2083$ Å in this cell.

An interesting aspect of the results is shown in Figure 2.6. Even for a timestep and density convergence criterion small enough so that the first few collision peaks show elastic collisions and therefore energy conservation, after a few periodic collisions, the two atoms stop colliding. This is because after a certain amount of time, the velocity gains components in x- and y-direction, even though the starting momentum was only in z-direction. Most likely this is due to numerical errors adding up over time. An example of the change of the x, y and z velocity components over time is shown in Figure 2.7 for the first C atom, and in Figure 2.8 for the second C atom. This effect can be observed for all choices of density convergence criterion and timestep, and is shown here to explain why there is only ever a certain amount of peaks in the following energy plots (Figure 2.9 – Figure 2.14).

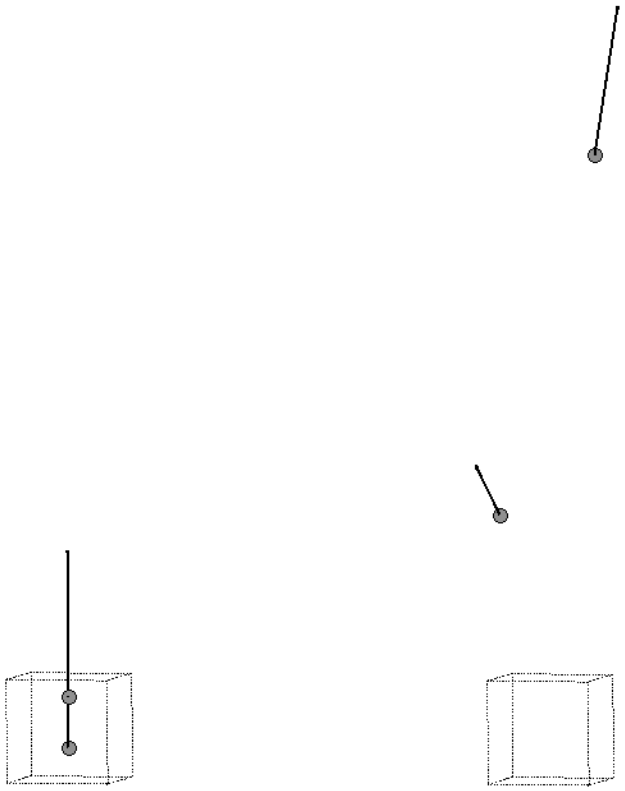

(a) The system after 0 fs.

(b) The system after 400 fs.

Figure 2.6: Two carbon atoms in a cell with periodic boundary conditions. The arrows indicate velocities. The initial kinetic energy was 22 eV, the timestep 0.1 fs.

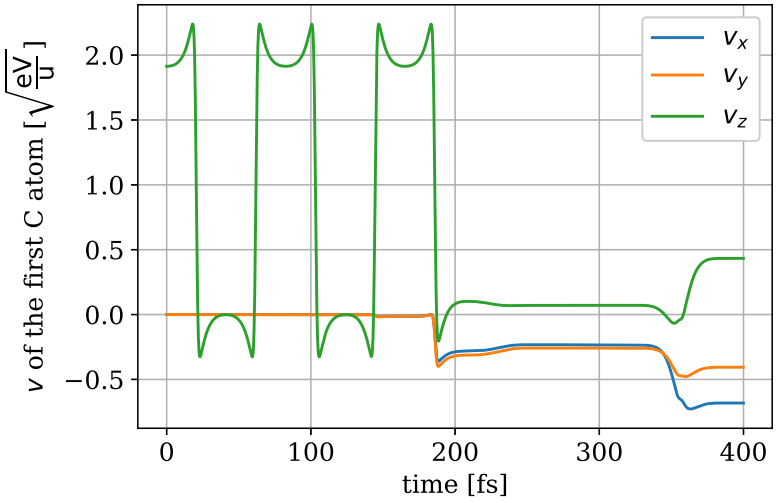

Figure 2.7: The velocity components of the second C atom over time, for a starting energy of 22 eV and a timestep of 0.1 fs.

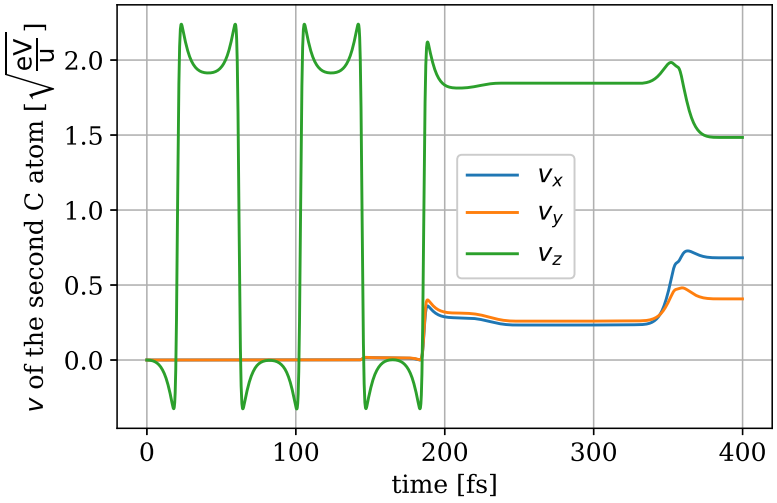

Figure 2.8: The velocity components of the first C atom over time, for a starting energy of 22 eV and a timestep of 0.1 fs.

2.4.1 Choosing the Timestep

The effect of the timestep on atomic trajectories and energy conservation has been tested in simulations of a head-on collision of two carbon atoms. The initial kinetic energy of the first C atom was set either to 22 or 100 eV, while the second C atom was at rest.

An initial kinetic energy of 22 eV

Figure 2.9 shows variation of the kinetic energy of two C atoms with time in the simulation of their head-on collision, where the initial kinetic energies of atoms were set to 22 eV and 0 eV.

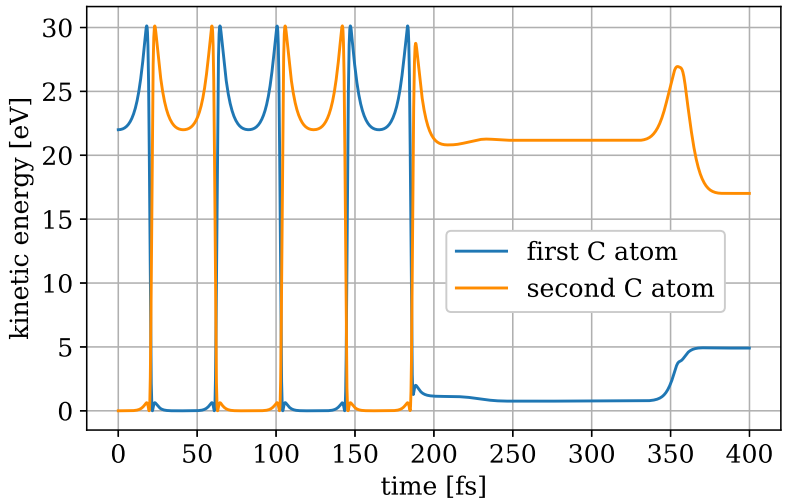

Figure 2.9: Variation of the kinetic energy of two carbon atoms in a simulation of their head-on elastic collision. The initial kinetic energies of the atoms was set to 22 eV and 0 eV, and the timestep was set to 0.1 fs

For timesteps of 0.1, 0.5 and 1.0 fs, the resulting energies look similar as in Figure 2.9. Before the 5^{th} collision (at about 175 fs), the peaks of the kinetic energy are at the same level (Table 2.2), thus confirming that this is an elastic collision. After the 5^{th} collision, the x- and y-components of the velocity become large enough so that the next collision does not take place. (see Figure 2.7 and Figure 2.8).

On the other hand, for timesteps of 1.5 and 2.0 fs, the energies are far less-well conserved for a starting energy of 22 eV (Figure 2.10 and Figure 2.11). Therefore, for an initial ion energy of around 22 eV, the timestep should not be chosen to be larger than 1 fs.

More grid points For a starting energy of 22 eV, a timestep of 0.1 fs, and a density convergence criterion of 10^{-5}, a simulation was done with increased number of grid points

gpts = (56 × 56 × 56) (grid spacing $h \approx 0.1786$ Å) instead of gpts = (48 × 48 × 48) ($h \approx 0.2083$ Å). Figure 2.12 shows that in this case, the kinetic energy stays well-conserved until the 7$^{\text{th}}$ collision, instead of the 5$^{\text{th}}$. However, there is no great difference in how well the peaks align with each other.

Table 2.2: The difference [eV] of the second, third and fourth energy peaks to the first energy peak, of the first C atom for an initial energy $E_{in} = 22$ eV. The case where the timestep $dt = 0.1$ fs and the density convergence criterion is 10^{-5} is shown in Figure 2.9.

density convergence	0.1 fs	0.5 fs	1.0 fs	1.5 fs
10^{-4}	0.0007	−0.0101	0.0006	−0.2427
	−0.0053	−0.0329	0.0555	−0.2566
	0.0031	−0.0544	0.0344	9.8516
10^{-5}	−0.0034	0.0060	0.0219	−0.2140
	−0.0079	−0.0226	0.1035	−0.2420
	−0.0022	−0.0170	0.1387	7.0957

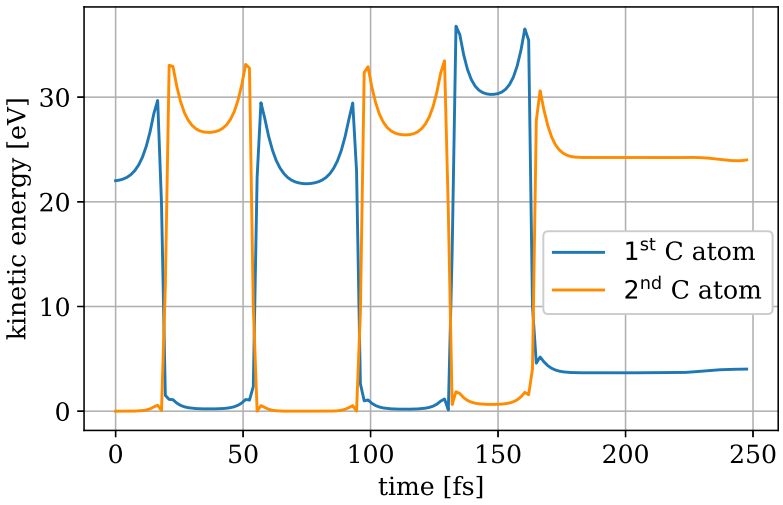

Figure 2.10: The kinetic energy of the two C atoms over time for a starting energy of 22 eV and a timestep of 1.5 fs.

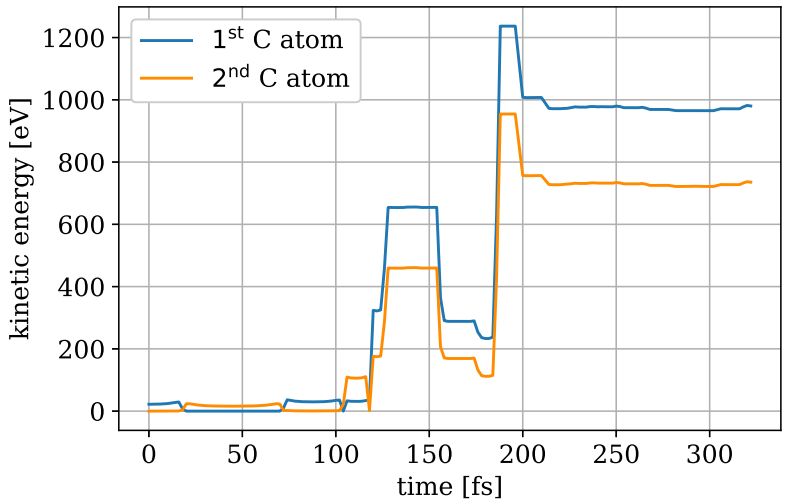

Figure 2.11: The kinetic energy of the two C atoms over time for a starting energy of 22 eV and a timestep of 2.0 fs.

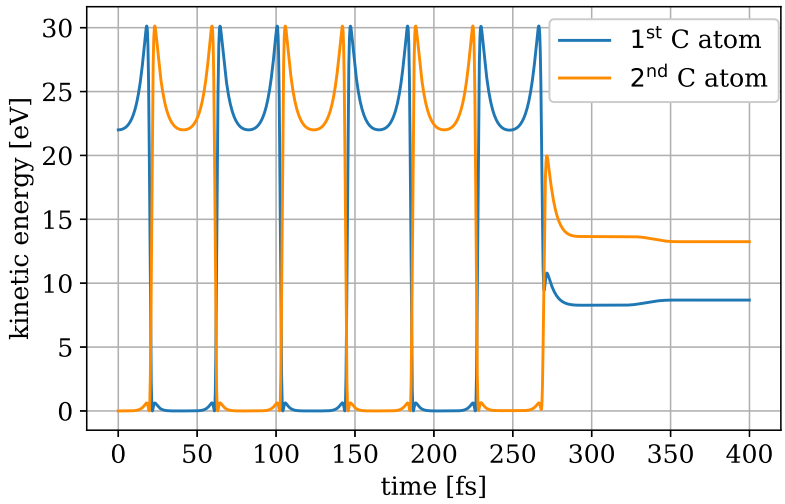

Figure 2.12: The kinetic energy over time for a starting energy of 22 eV, a timestep of 0.1 fs, and grid spacing $h \approx 0.1786$ Å.

An initial kinetic energy of 100 eV

For an initial kinetic energy of 100 eV, a smaller timestep is necessary to have an energy that is as well-conserved as with 22 eV. As shown in Figure 2.13 and Figure 2.14, a timestep of 0.5 fs is now needed to reach a reasonably converged kinetic energy, whereas for 22 eV, a timestep of 1.0 fs was small enough. As for the lower energy case, the atoms still drift apart after the 5^{th} collision.

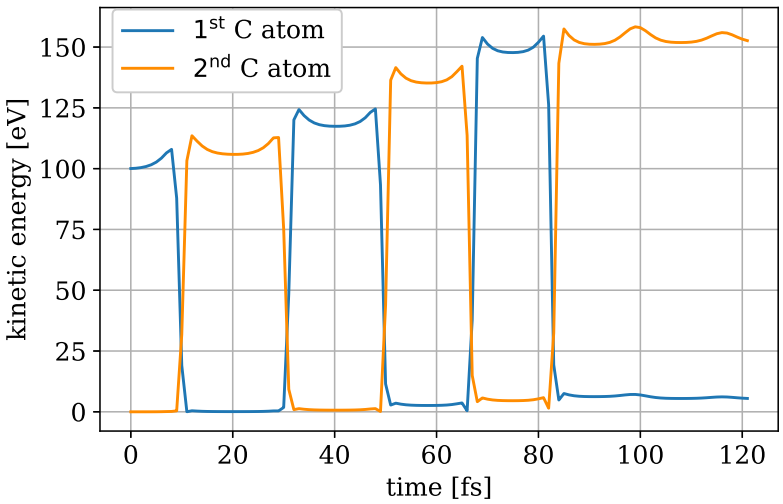

Figure 2.13: The kinetic energy over time for a starting energy of 100 eV and a timestep of 1.0 fs.

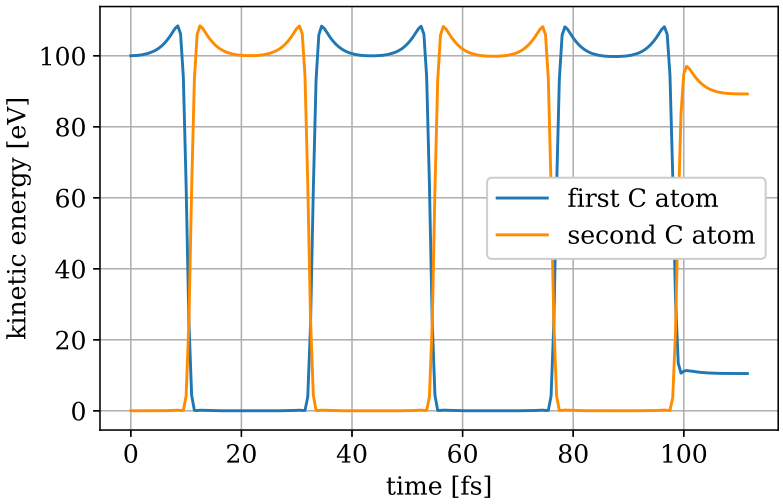

Figure 2.14: The kinetic energy over time for a starting energy of 100 eV and a timestep of 0.5 fs.

Additionally, it was tried to use an adaptive timestep, so that the distance, $ds = v \cdot dt$, overcame by an atom during one timestep is independent of its velocity. This approach, however, has not been further used in the simulations of ion implantation, but the test simulations are described in the Supplement 5.

In summary, a timestep as large as 1 fs is sufficient to allow physical results, if the atoms move at low velocities. Larger timesteps than that, such as $dt = 1.5$ fs lead to collisions that are no longer elastic, either because the atoms move too close to each other before the forces can push them apart, thus causing energy not to be conserved, or due to numerical errors in the integration of the equations of motion. If the velocities are higher such that the corresponding C kinetic energy reaches magnitudes of about 100 eV, a timestep of 0.5 fs is needed to achieve elastic collisions. The density convergence criterion has only a small effect on these tests. Unless specified otherwise, a timestep of $dt = 1$ fs and a density convergence criterion of $5 \cdot 10^{-5}$ were used for further simulations.

3 Results and Discussion

For the main part of this study, a graphene layer consisting of 162 C atoms was simulated in a 22.23×22.23 Å xy-plane with 120° and 60° angles. The cell was 40 Å high in the perpendicular z-direction for the cases where the initial energy of the ion was below 100 eV. For higher energies, the ejected C atom tended to reach the next periodic layer of graphene before it was clear whether or not the ion implants. Therefore, for higher energies, the cell was was given a height of up to 100 Å in z. For the simulations, a k-point mesh of $3 \times 3 \times 1$, a density convergence criterion of $5 \cdot 10^{-5}$, and LCAO mode with PBE and dzp basis were used.

3.1 Binding Energies of Heteroatoms in Graphene

The binding energy in graphene was calculated for each examined element, in order to compare the results to literature values and provide equilibrium geometries of the substitutions. For this purpose, a system where a heteroatom is incorporated in a graphene layer was simulated and relaxed. The grid spacing was chosen as $h = 0.18$ Å, and spin polarization was taken into account for all calculations. The BFGS optimization algorithm was used to relax the systems, such that the force on any individual atom was less than 0.02 eV/Å for convergence.[53]

The binding energy E_{bind} was calculated using the formula

$$E_{bind} = E_{sub} - (E_{vac} + E_{het}) \ , \tag{3.1}$$

where E_{sub} is the energy of a graphene sheet doped with a heteroatom which replaces one or two C atoms, E_{vac} is the energy of a graphene sheet with a mono- or divacancy, and E_{het} is the energy of only the heteroatom.

The binding energy was examined for two cases: the case where the heteroatom replaces one C atom in the lattice, and the case where the heteroatom replaces two C atoms in the lattice. For each of the two cases, three systems were needed to calculate the binding energy:

(a) Graphene layer with a mono-/divacancy with no heteroatom (Figure 3.1a)
Fermi-Dirac Smearing was used with a width of 0.025 eV, and the energy of the relaxed system E_{vac} was calculated.

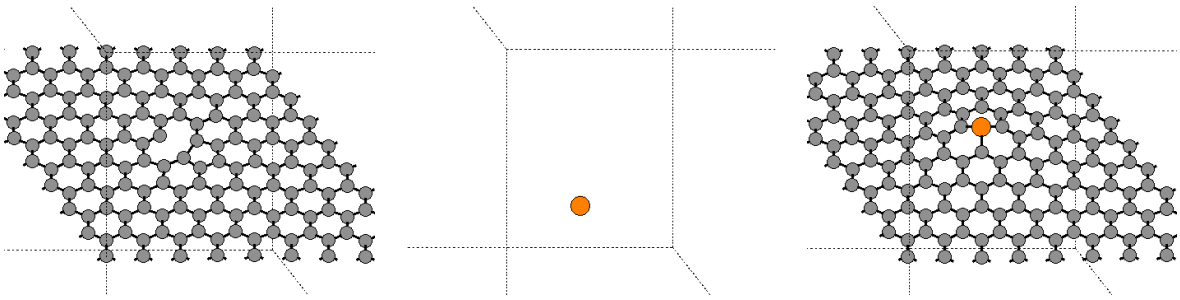

(a) Graphene with vacancy. (b) Only the heteroatom. (c) Incorporated heteroatom.

Figure 3.1: The three geometries that were used to obtain the binding energies.

(b) Only the heteroatom (Figure 3.1b)
This system is not a periodic structure, so only one k-point was used, and it obviously did not need to be relaxed, as it only consists of one atom. The total magnetic moment was fixed to the initial value according to Hund's rule, and Fermi-Dirac smearing was set to a width of 0.0 eV. An exception had to be made for the Ni atom: for Ni, Fermi-Dirac smearing was set to a width of 0.2 eV, because otherwise the calculation did not converge. The energy of the single heteroatom E_{het} was calculated.

(c) Heteroatom incorporated in the monovacancy/divacancy (Figure 3.1c)
Initially, the heteroatom was elevated slightly out of plane in z-direction, and Fermi-Dirac smearing was used with a width of 0.025 eV. The total energy of the relaxed system E_{impl} was calculated.

The calculated binding energies of different elements in graphene are shown in Table 3.1 and compared with the results by Pašti et al.,[58] that were obtained with the same PBE functional but with the use of the plane-wave basis set. The optimized geometries of different heteroatoms incorporated in a mono- and divacancy are shown in Figure 3.2 and Figure 3.3 respectively.

Table 3.1: Calculated binding energies [eV] of heteroatoms in graphene in mono- and divacancy configurations, and literature values for the monovacancy case.

heteroatom	divacancy	monovacancy	Pašti et al.[58]
B	−7.680	−12.502	−12.91
C	−7.544	−15.227	−15.69
N	−7.227	−11.764	−12.02
Al	−4.796	−5.534	−5.15
Si	−7.091	−8.419	−8.21
P	−6.640	−8.262	−8.31
Mn	−4.496	−6.270	−6.18
Ni	−6.344	−7.035	−6.64
Ge	−5.054	−6.494	−6.30

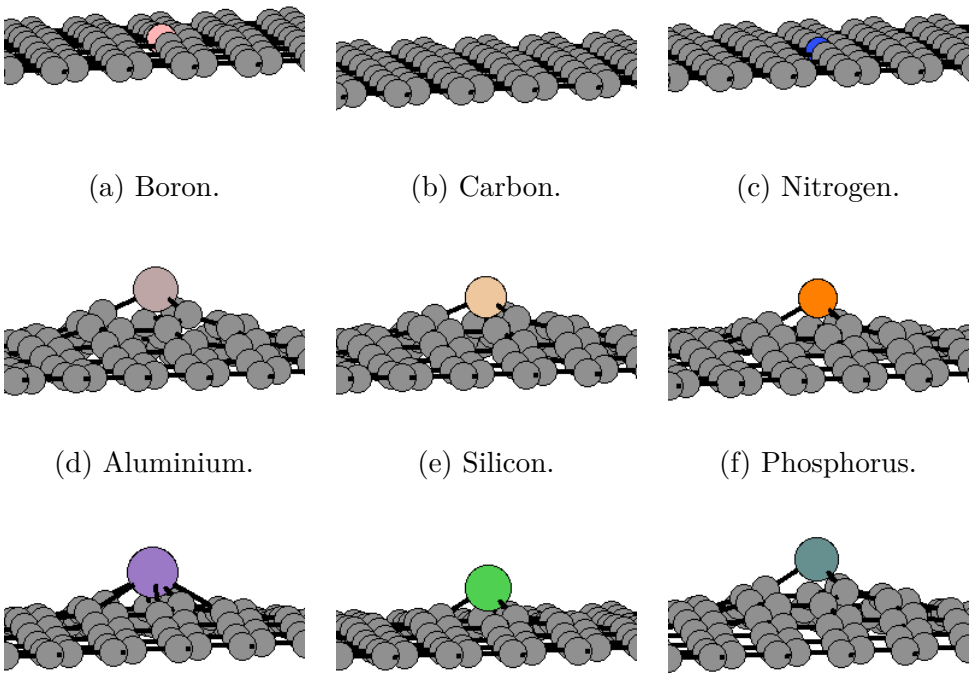

(a) Boron. (b) Carbon. (c) Nitrogen.

(d) Aluminium. (e) Silicon. (f) Phosphorus.

(g) Manganese. (h) Nickel. (i) Germanium.

Figure 3.2: The optimized structures of heteroatoms substituting one C atom in the graphene lattice.

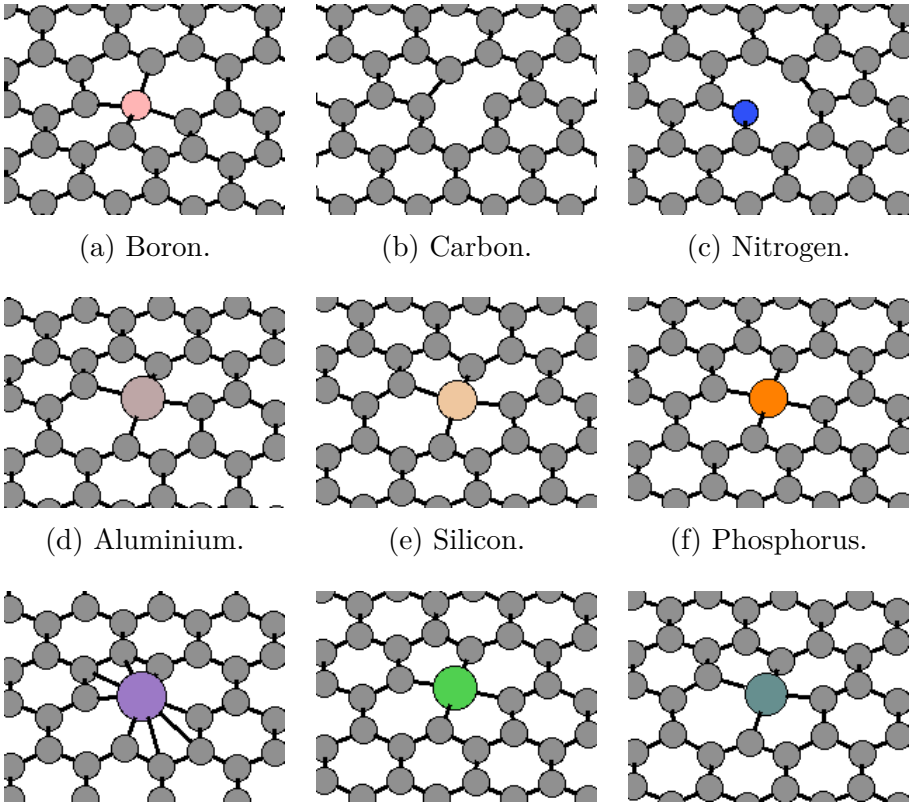

(a) Boron. (b) Carbon. (c) Nitrogen.

(d) Aluminium. (e) Silicon. (f) Phosphorus.

(g) Manganese. (h) Nickel. (i) Germanium.

Figure 3.3: The optimized structures of heteroatoms substituting two C atoms in the graphene lattice.

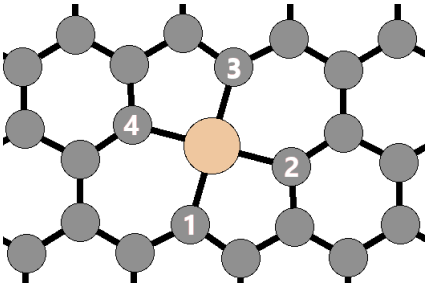

Figure 3.4: Top-view of graphene with a Si atom implanted in a divacancy. The four C atoms bonded to the Si are numbered to allow them to be referenced.

The way the ions are incorporated in a divacancy was examined further for all the ions that substitute for two C atoms. Firstly, the average z-position of all C-atoms was subtracted from the z-position of the ion to get a measure for how much the ion sticks out from the lattice (Δion). Additionally, the z-position of the ion is subtracted from the z-positions of its four C neighbours (labelled 1 – 4 in Figure 3.4). The results are shown in Table 3.2, where Δion shows by how much the ion protrudes from the graphene layer, and C_1 – C_4 show how much difference there is in z-position between the ion and the respective C atom as shown in Figure 3.4.

Table 3.2: Difference in z-position between the ion and the average of all C atoms Δion[Å], and difference in z-position between the ion and its four neighbours C_1 – C_4 [Å], as marked in Figure 3.4.

heteroatom	Δion	C_1	C_2	C_3	C_4
B	0.04	0.33	−0.35	0.34	−0.34
Al	0.71	−0.39	0.14	−0.43	0.08
Si	0.11	−0.31	0.29	−0.31	0.28
P	0.12	0.00	−0.01	−0.01	0.00
Mn	0.79	−0.58	−0.58	−0.58	−0.58
Ni	0.28	−0.09	−0.10	−0.10	−0.09
Ge	0.34	−0.38	0.30	−0.41	0.28

When looking at the relaxed structures of a heteroatom incorporated in a divacancy (Figure 3.3), it can be seen that the heteroatom and its four neighbours are often slightly out-of-plane. This is quantified in Table 3.2, where it can be seen that the heteroatoms are up to 0.8 Å out-of plane. In most cases, two of their neighbouring C atoms on opposite sides of the heteroatom have a higher z-position, while the other two C neighbours have a lower z-position. P is an exception, in that all for of its neighbours appear to be in almost exactly the same z-position as the P ion. For Ni and Mn, all four neighbours are out-of-plane, but all in the same direction instead of half going up and half going down. C and N were not examined, since they substitute for only one C atom, and leave a monovacancy.

For most ions, the C neighbours alternately lie above and below the impurity, creating a tetrahedal-like geometry, and for some ions the C neighbours protrude out of the plane in the same direction, creating a pyramidal-like geometry. The elevation of the Al ion is higher than expected. As a test, the calculation was repeated for Al with an initial geometry closer to the tetrahedal one, and the result remained the same.

3.2 Choice of Computational Parameters

To find out how the choice of computational parameters affects the results of the simulations, some additional test calculations were performed for implantation of Al, Si and Ge atoms, namely head-on collision simulations were done with different density convergence criteria and timesteps.

3.2.1 Silicon

For Si, it was first tested how different the kinetic energies of the Si atom and of the ejected C atom would be for different parameters after 160 fs (Table 3.3 and Table 3.4). The initial energy of the Si atom was 14 eV. The energies of the Si atom and the ejected C atom can be seen for one case in Figure 3.5. The time of 160 fs after starting the simulation was chosen because at this point, it is clear whether the ion will implant in the lattice (Figure 3.5 and Figure 3.6).

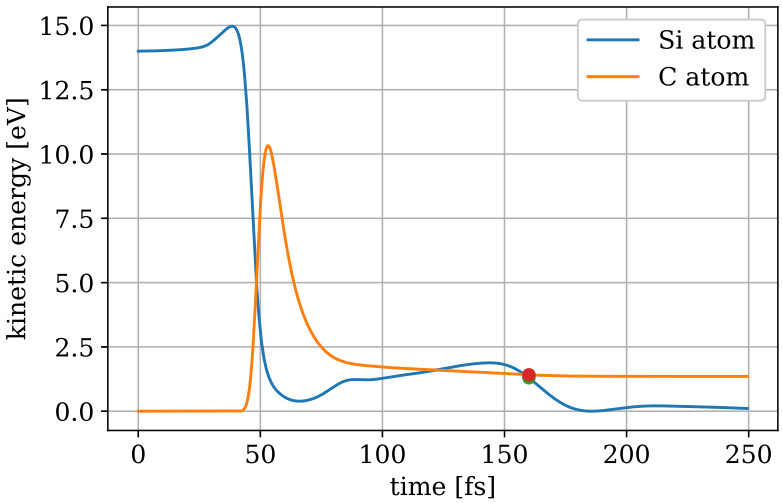

Figure 3.5: Kinetic energy of the Si atom and the C atom that it hits for a starting energy of 14 eV, a density convergence criterion of 10^{-4} and a timestep of $dt = 0.5$ fs. The timestep at 160 fs is marked with a dot.

Table 3.3 and Table 3.4 show that there are only small differences in energy for the different parameters. However, this method of comparing simulations is not ideal, because what is of interest here is not the energy after a certain time, but rather whether or not the initial energy is enough to replace a C atom in the lattice, and this is what should be accurate for the chosen parameters.

Therefore, to ascertain whether different parameters give similar results, the minimum energy the Si atom must have in order to eject the C atom it hits from the lattice was

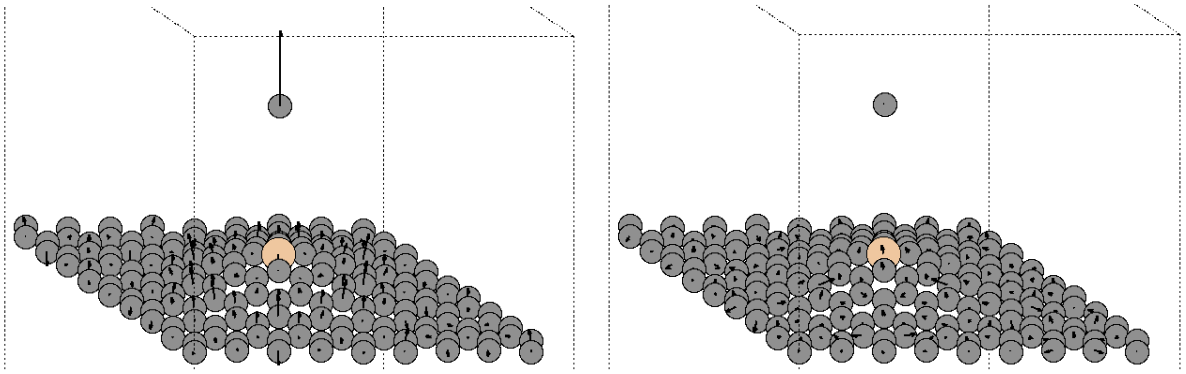

(a) Arrows indicate velocities. (b) Arrows indicate forces.

Figure 3.6: The state of the system after 160 fs if Si has an initial kinetic energy of 14 eV. The grey spheres correspond to C atoms, the orange sphere to the Si atom.

Table 3.3: Energy [eV] of the Si atom after 160 fs.

density convergence	0.1 fs	0.3 fs	0.5 fs	1.0 fs
10^{-4}	1.321	1.269	1.299	1.313
$5 \cdot 10^{-5}$		1.332	1.344	
10^{-5}	1.345	1.338	1.315	1.270

Table 3.4: Energy [eV] of the C atom after 160 fs.

density convergence	0.1 fs	0.3 fs	0.5 fs	1.0 fs
10^{-4}	1.751	1.760	1.299	1.415
$5 \cdot 10^{-5}$		1.391	1.209	
10^{-5}	1.375	1.367	1.389	1.399

compared for different parameters. Assuming that the smallest timestep and electron density convergence criterion give the most accurate result, if larger timesteps and less demanding density convergence give a very similar result, then that is a good indicator that these values can be used to speed up the calculations without great loss of accuracy. For this purpose, the minimum energy needed for Si implantation was determined to within a precision of 0.25 eV even though for practical purposes, this would be unnecessarily precise.

To find the minimum initial kinetic energy of a Si ion $E_{in} = E_{min}$ needed to make C leave the lattice, the simulations were done for different energies E_{in}, checking each time whether or not the C atom has escaped the lattice. Table 3.5 shows the tipping point: for the lower respective energy in each field, C does not get ejected, and for the higher one, it does get ejected and the Si atom gets implanted into the lattice.

Table 3.5: Initial kinetic energy [eV] of Si atom needed to eject the C atom from the lattice in a head-on collision. For the first value, C does not escape, and for the second, it does.

density convergence	0.1 fs	0.3 fs	0.5 fs	1.0 fs
10^{-4}	[13.00, 13.25]	[13.25, 13.50]	[13.25, 13.50]	[13.50, 13.75]
$5 \cdot 10^{-5}$	[13.25, 13.50]	[13.50, 13.75]	[13.50, 13.75]	[13.50, 13.75]
10^{-5}	[13.25, 13.50]	[13.25, 13.50]	[13.25, 13.50]	[13.25, 13.50]

Another important factor for choosing a set of parameters is how much of a difference they make in terms of simulation time. Therefore, the time needed to simulate 200 fs is determined from the outputs, by checking how much time has passed between the first timestep and the timestep corresponding to 200 fs. The time it took to simulate 200 fs is shown in Table 3.6; this was chosen because after this time, the Si atom has been clearly implanted into the graphene lattice. (Figure 3.7 and Figure 3.8.)

As seen in Table 3.5 and Table 3.6, the difference in results for the different timesteps and density convergence criteria is less than 1 eV. However, the simulation time in CPU-hours ranges from less than 400 h to over 4000 h. Clearly, much can be gained from a sensible choice of parameters. Subsequently, similar tests of parameters were carried out for an Al ion and a Ge ion, to see if different ion mass and electron configuration has an impact on the viability of certain parameters.

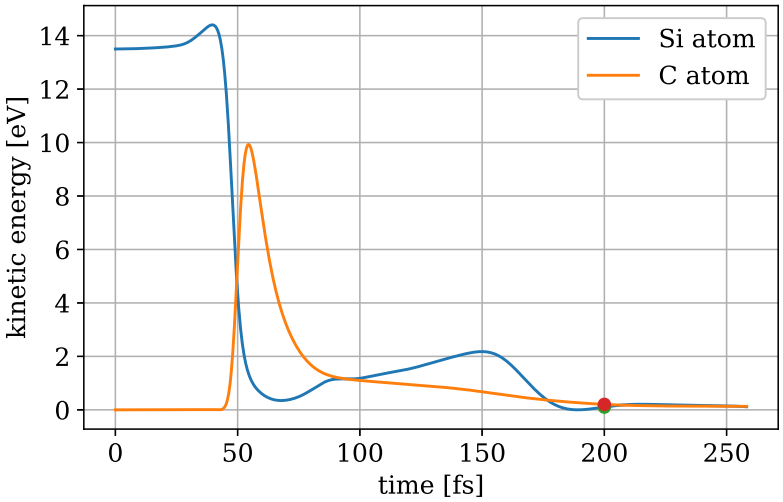

Figure 3.7: Kinetic energy for the case where the Si atom has an initial energy of 13.5 eV. The density convergence criterion is 10^{-5} and one timestep is 0.1 fs. The timestep of 200 fs is marked with a dot.

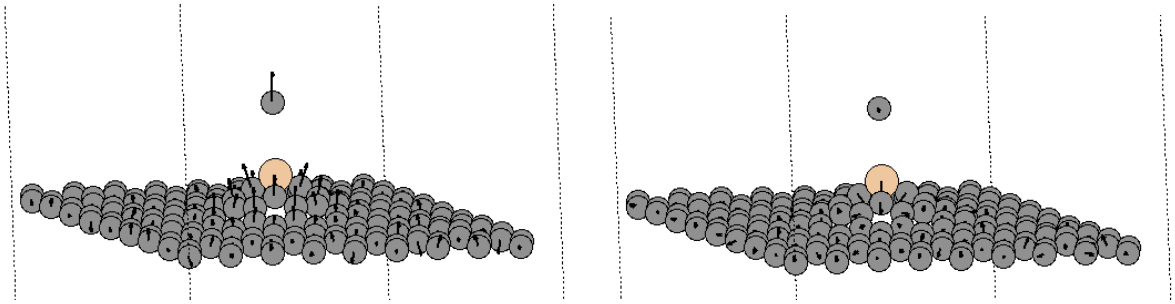

(a) Arrows indicate velocities.

(b) Arrows indicate forces.

Figure 3.8: The state of the system after 200 fs if Si has an initial energy of 13.5 eV. The grey spheres correspond to C atoms, the orange sphere to the Si atom.

Table 3.6: CPU-time [h] required to simulate 200 fs for different combinations of computational parameters and initial kinetic energy of the Si ion of 13.5 eV. The numbers in parentheses are added for the cases where the C atom does not escape for 13.5 eV as seen in Table 3.5, corresponding to an initial energy of 13.75 eV instead.

density convergence	0.1 fs	0.3 fs	0.5 fs	1.0 fs
10^{-4}	3233	1306	611	383 (405)
$5 \cdot 10^{-5}$	3219	1412 (1399)	916 (968)	423 (440)
10^{-5}	4238	1809	844	540

The maximum implantation energy E_{max} was found by finding the maximum initial kinetic energy that still allows the ion to implant and not be transmitted through the lattice. The E_{max} was also tested for several different timesteps, because the higher velocity of the ion means that a smaller timestep might be necessary, as the ion covers greater distances in one timestep. For the density convergence criterion a value of $5 \cdot 10^{-5}$ was chosen, as Section 3.2.1 has shown this to be a good balance of computational time and accuracy. An accuracy of 1 eV was deemed enough for the maximum implantation energy. The results are shown in Table 3.7. They don't have a strong dependence on the timestep, therefore a timestep of 1 fs can reasonably be chosen.

Table 3.7: Initial energy [eV] of Si atom needed to be transmitted through the lattice in a head-on collision. For the first value, Si implants, and for the second, it goes through. The density convergence criterion is $5 \cdot 10^{-5}$.

0.25 fs	0.5 fs	1.0 fs
[144, 145]	[144, 145]	[145, 146]

Finite differences (FD) calculations were performed for Si to compare the results of the FD method and the LCAO method. As the calculations take much longer with the FD method, only the head-on and the hexagon-center impact points were tested, using a timestep of 1.0 fs and a density convergence criterion of $5 \cdot 10^{-5}$. The results are shown in Table 3.8, along with the results from the LCAO method for comparison. The LCAO results differ from the FD results by 2 – 4 eV. Where each LCAO calculation took about 400 or 500 CPU-hours, each FD calculation took around 40 000 CPU-hours.

Table 3.8: Minimum E_{min} and maximum E_{max} initial kinetic energies [eV] of the Si ion that will lead to an implantation for a head-on collision, and minimum energy the ion needs to be transmitted through the lattice (E_{trans}) at the center of a graphene hexagon, obtained with the FD and the LCAO methods.

impact point	E_{min}[eV]	E_{max}[eV]	E_{trans}[eV]
	FD mode		
head-on	12	140	-
center of hexagon	-	-	27
	LCAO mode		
head-on	14	145	-
center of hexagon	-	-	29

3.2.2 Aluminium

As in Section 3.2.1, the goal is again to determine which timestep and density convergence criterion combination is needed to achieve a good balance between accuracy and computational time. It is important to check if the same parameters can be used for different elements, so here it is tested for Al which has a similar mass but a different valence configuration than Si. The minimum energy E_{in} that the Al atom must have in order to eject the C atom it hits in a head-on collision is found for different parameter combinations (Table 3.9.)

Note that C does not get ejected if the energy of the Al ion is increased by about $2-4$ eV from the energy given in this table. However, for higher energies, C is ejected again. The reason for this is presumably that in this small energy window of no implantation, Al is fast enough to knock out the C atom, but also fast enough to follow the C atom through the graphene layer for a small distance. The prolonged interaction between the Al atom and the C atom causes the C atom to be pulled back to the lattice instead of escaping, knocking the Al atom back out of the lattice. This behaviour was observed for all tested sets of parameters.

Table 3.9: Initial energy [eV] of Al atom needed to eject the C atom from the lattice. For the first value, C does not escape, and for the second, it does.

density convergence	0.1 fs	0.25 fs	0.5 fs	1.0 fs
10^{-4}	$[18.00, 18.25]$	$[18.00, 18.25]$	$[18.25, 18.50]$	$[18.50, 18.75]$
$5 \cdot 10^{-5}$	$[18.25, 18.50]$	$[18.25, 18.50]$	$[18.25, 18.50]$	$[18.25, 18.50]$
10^{-5}	$[18.25, 18.50]$	$[18.25, 18.50]$	$[18.25, 18.50]$	$[18.25, 18.50]$

CPU-time needed to simulate a certain period of time with different sets of computational parameters is shown in table Table 3.10. In this case a time period of 250 fs was chosen because after this time it was clearly visible that the C atom was being ejected and not becoming an adatom (see Figure 3.9 and Figure 3.10). As can be seen from Table 3.10 and Table 3.10, the kinetic energy of the Al ion at which the C atom is ejected stays very consistent, however computational time strongly depends on the chosen parameters.

Table 3.10: CPU-time [h] required to simulate 250 fs for different combinations of computational parameters and initial kinetic energy of the Al ion of 18.5 eV. The numbers in parentheses are added for the cases where the C atom does not escape for 18.5 eV as seen in Table 3.9, corresponding to an initial energy of 18.75 eV instead.

density convergence	0.1 fs	0.25 fs	0.5 fs	1.0 fs
10^{-4}	3863	1829	1064	447 (484)
$5 \cdot 10^{-5}$	3954	1962	1130	508
10^{-5}	5300	2621	1542	647

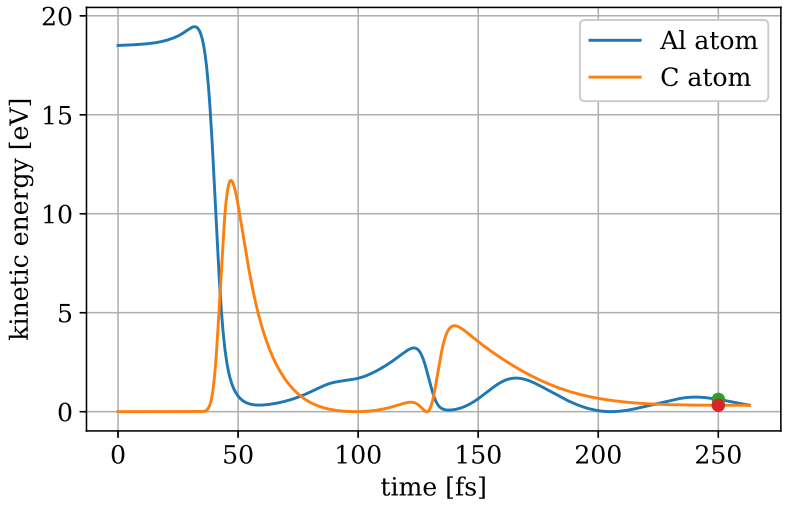

Figure 3.9: Kinetic energy for the case where the Al atom has an initial energy of 18.5 eV. The density convergence criterion is 10^{-5} and one timestep is 0.1 fs. The timestep of 250 fs is marked with a dot.

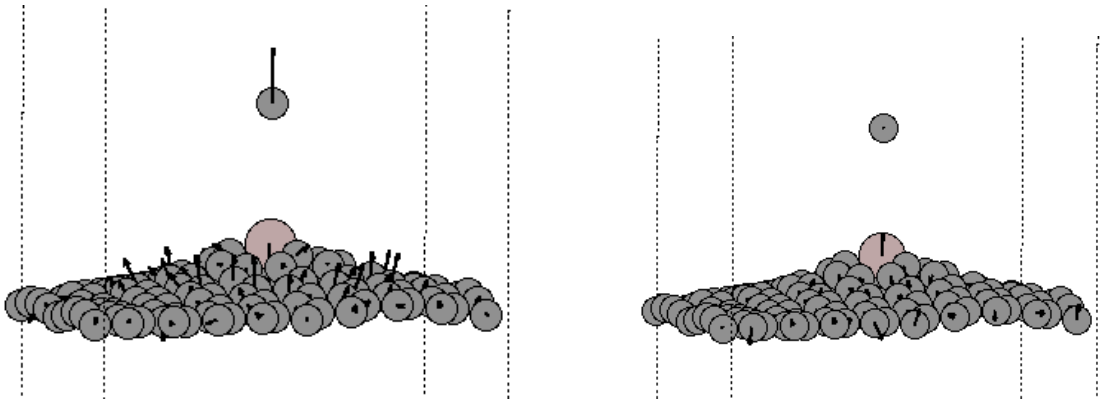

(a) Arrows indicate velocities. (b) Arrows indicate forces.

Figure 3.10: The state of the system after 250 fs if Al has an initial energy of 18.5 eV. The grey spheres correspond to C atoms, the pink sphere to the Al atom.

3.2.3 Germanium

As in Section 3.2.1 and Section 3.2.2, the minimum implantation energy E_{min} is determined for different computational parameters. Ge is heavier than Si or Al, therefore it may behave differently and need different parameters. The minimum energy Ge needs to eject C from graphene upon a head-on impact is shown in Table 3.11.

As described for Al in Section 3.2.2, Ge also has a small energy range where C is not ejected if the energy of Ge is a few eV higher than the minimum implantation energy.

Table 3.11: Initial energy [eV] of Ge atom needed to eject the C atom from the lattice. For the first value, C does not escape, and for the second, it does.

density convergence	0.1 fs	0.25 fs	0.5 fs	1.0 fs
10^{-4}	[23.00, 23.25]	[22.25, 22.50]	[23.00, 23.25]	[23.25, 23.50]
$5 \cdot 10^{-5}$	[22.75, 23.00]	[23.00, 23.25]	[23.00, 23.50]	[23.25, 23.50]
10^{-5}	[23.00, 23.25]	[23.00, 23.25]	[22.75, 23.25]	[23.00, 23.25]

To check how much of a difference the timestep and density convergence criterion make in terms of computational time, the time it takes to simulate 250 fs is compared for the different parameters in Table 3.12. As before, the simulation time of 250 fs was chosen because at this time the C atom has been clearly ejected from the lattice (see Figure 3.11 and Figure 3.12).

Table 3.12: CPU-time [h] required to simulate 250 fs for different combinations of computational parameters and initial kinetic energy of the Ge ion of 23.5 eV for different computational parameters. The numbers in parentheses are added for the cases where the C atom does not escape for 23.5 eV as seen in Table 3.11, corresponding to an initial energy of 22.5 eV instead.

density convergence	0.1 fs	0.25 fs	0.5 fs	1.0 fs
10^{-4}	3799	1264 (1698)	1097	473
$5 \cdot 10^{-5}$	3989	1995	1182	526
10^{-5}	5325	2568	1536	670

Based on all these tests with Si, Al, and Ge, a density convergence criterion of $5 \cdot 10^{-5}$ and a timestep of 1 fs were chosen for simulations of ion implantation. The only exceptions were cases with a very high initial kinetic energy, and all calculations involving N. In these cases, a smaller timestep was used.

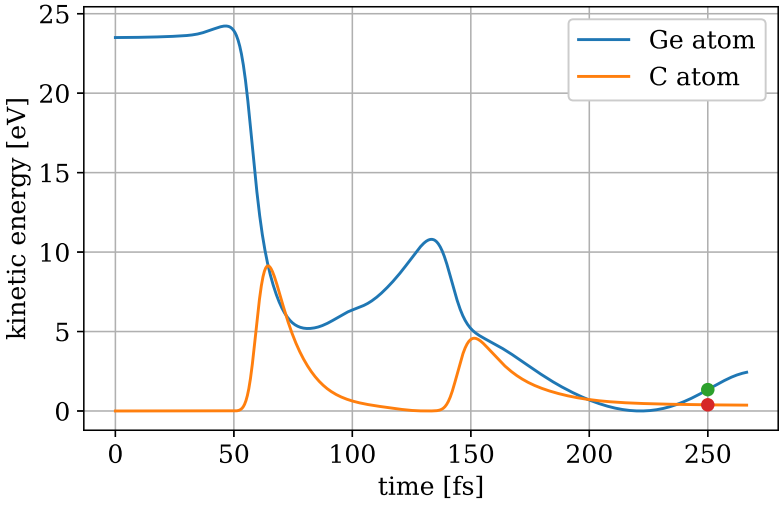

Figure 3.11: Kinetic energy for the case where the Ge atom has an initial energy of 23.5 eV. The density convergence criterion is 10^{-5} and one timestep is 0.1 fs. The timestep of 250 fs is marked with a dot.

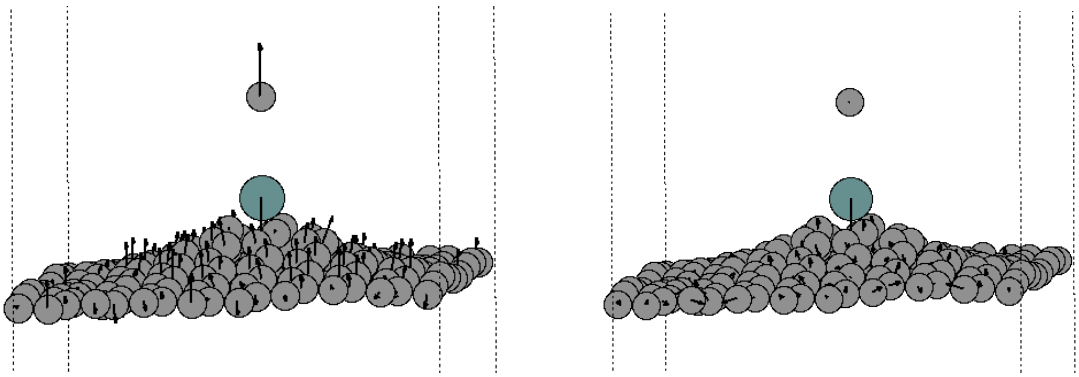

(a) Arrows indicate velocities.

(b) Arrows indicate forces.

Figure 3.12: The state of the system after 250 fs if Ge has an initial energy of 23.5 eV. The grey spheres correspond to C atoms, the green sphere to the Ge atom.

3.3 Ion Implantation

In the analysis of the results of ion implantation simulations, a successful implantation event has been determined by two main conditions: incorporation of an ion into the lattice and sputtering of one or more C atoms. Events where a C atom escapes from the lattice but remains in the structure as an adatom were not considered as implantation. A study has shown that for Ge at room temperature, configurations where an ion is implanted but the C remains as a nearby adatom spontaneously relax such that the result is non-defective graphene and the ion as an adatom.[26]

Stability of such structures was also tested in this work for individual simulations with B, N, Si, P, Mn, and Ni by extending simulations for a longer time after an ion got implanted but a C atom remained in the structure as an adatom. In many cases it was observed that the C adatom indeed replaces the heteroatom. However, for some impurities, such as B, N and Si, the replacement was never observed during the simulation time. Nevertheless, for consistency of results, the cases where C came back were classified as cases where the initial energy was too low to facilitate implantation.

3.3.1 Head-On Impact Point

Table 3.13 shows the minimum initial energy the ion needs to have in order to eject a C atom, which it hits head-on (see Figure 1.1a). It also shows the maximum initial energy the ion can have so that it is not transmitted through the graphene layer and escape. In other words, for any initial energy between E_{min} and E_{max}, the ion ejects one C atom and implants in the resulting monovacancy. Cases where the C atom was almost ejected and it looks like the ion implanted in the lattice, but then the C-atom is pulled back, were not counted as implantations. E_{max} is not given for some heteroatoms: the reason is that for these atoms, no instance of the ion going through the lattice could be observed for any initial energy, where the highest initial energy that was tried was 500 eV. This happens for ions with a mass similar to C, and so according to Figure 1.2, they transfer almost all of their kinetic energy to the C atom, and so the ion has no kinetic energy left with which to escape the lattice. For N, attempting to implant it with an initial energy lower than 11 eV may result in implantation of the N ion without sputtering any C atom, so that the C atom becomes an adatom.

The displacement threshold energy in graphene is 21.14 eV,[62] yet in the head-on collisions, the energy transferred to a C atom by an ion with minimum implantation energy can be significantly lower than this value. This may be due to chemical interactions between the incoming ion and the C atoms neighbouring the displaced C atom.

As can be seen in Table 3.13, lighter ions tend to have a larger energy window than heavier ones, probably due to the mass-energy transfer peak for head-on collisions with similar mass shown in Figure 1.2. In cases where heteratoms have similar masses, C has a larger energy window than B and N, and Si larger than Al and P, which suggests

Table 3.13: Minimum E_{min} and maximum E_{max} initial kinetic energy [eV] of the ion that results in the implantation for the case of a head-on collision. M_{ion} is the atomic mass of the element that was implanted, and R_{vdW} is its van der Waals radius.[59–61]

ion	M_{ion}[u]	R_{vdW}[pm]	E_{min}[eV]	E_{max}[eV]
B	11	192	10	-
C	12	170	6	-
N	14	155	11	-
Al	27	184	19	112
Si	28	210	14	145
P	31	180	12	116
Mn	55	245	25	40
Ni	59	163	21	45
Ge	73	211	24	40

that the energy window in the head-on case is larger for heteroatoms that have the same number of valence electrons as the C atom they replace.

Interestingly, it has been found that there is a correlation between the minimum implantation energies and the calculated binding energies of the corresponding heteroatoms (Table 3.1), which can be seen in Figure 3.13. A possible explanation of this phenomenon is that elements that interact stronger with graphene, i.e. have lower binding energy, have a stronger effect on the weakening of the interaction between the knocked C atom and its neighbours in the lattice, which reduces the minimum sputtering energy of C. This, in turn, results in lowering of the minimum energy needed for implantation.

Tripathi et al.[26] used DFT-based molecular dynamics to simulate head-on collisions of Ge and a C atom in a graphene layer. Their result was $E_{min} = 26$ eV and $E_{max} = 42$ eV, which is close to the result that was obtained here ($E_{min} = 24$ eV and $E_{max} = 40$ eV).

3.3.2 Bond-Center Impact Point

If the ion impacts in the center of the bond between two C atom (Figure 1.1b), it usually ejects two C atoms (an example is shown in Figure 3.14) and then implants either in a divacancy, or, in the case of N and C, implants in place of one C atom, leaving a monovacancy empty. Table 3.14 shows the minimum and maximum implantation energies for an impact point in the center of the bond between two C atoms (Figure 1.1b).

The ion usually ejects two C atoms, but in some rare cases it was observed that only one C atom is sputtered, while the second one is attracted back to graphene. This happens only if the ions have low energies very close to E_{min}, and even then only rarely. In these cases, the ion implants in place of that one sputtered C atom, just as in Figure 3.2.

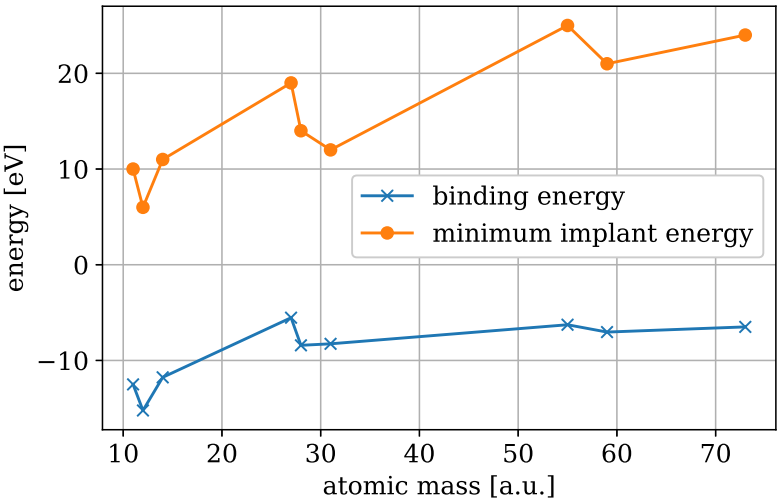

Figure 3.13: Binding energies in a monovacancy, and minimum implantation energies for a head-on impact of B, C, N, Al, Si, P, Mn, Ni and Ge. The continuous lines were added as a guide for the eye.

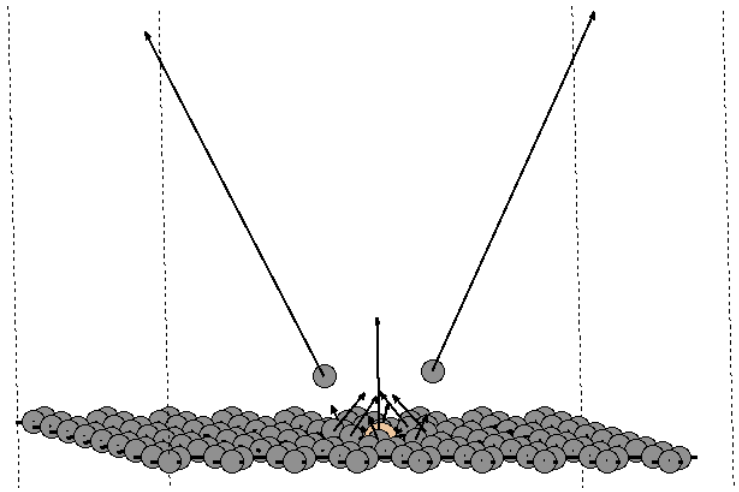

Figure 3.14: An Si atom ejecting two C atoms from graphene, after impacting in the center of the bond between two C atoms. This image shows the system after 45 fs. The arrows indicate velocities.

Table 3.14: Minimum E_{min} and maximum E_{max} initial kinetic energy [eV] of the ion that results in implantation in the case where the ion hits in the center of the bond between two C atoms.

ion	E_{min}[eV]	E_{max}[eV]
B	32	57
C	25	53
N	39	49
Al	29	92
Si	30	103
P	32	92
Mn	25	27
Ni	24	36
Ge	28	33

Curiously, for an initial energy of 32 eV, the Ge ion does not eject a C atom, even though it does for lower and higher energies. For C, the lowest energy for which implantation was observed was 25 eV, with one of the graphene atoms being ejected and the C ion implanting in the resulting monovacancy. However, for some higher initial energies such as 33 eV or 35 eV, none of the graphene C atoms get ejected. Then, for any energy $\geq$ 36 eV (but $\leq E_{max}$), two graphene C atoms get ejected, and the C ion implants in the resulting divacancy. For N, for an initial energy of 37 eV and 38 eV, N implants but the C atom is left as an adatom.

To compare binding energies and implantation energies, the minimum implantation energies were plotted in Figure 3.15, together with the binding energies from Section 3.1, shown in Table 3.1. No clear correlation, as in the case of a head-on impact point, can be seen.

Comparing the results for the head-on impact point and the bond-center impact point, it is of note that in general, more energy is needed to achieve implantation in the bond-center case. This makes sense, since in that case, the kinetic energy of the ion is transferred to two C atoms instead of just one. In the bond-center case, E_{max} exists for every heteroatom, even those that don't escape the lattice for high energies in the head-on case, and E_{max} is higher in the bond-center case. The reason for this is that for a sufficiently high energy, the incoming ion can simply pass between the two C atoms without removing them from the lattice, which is not possible for the head-on case. Combined, these effects lead to a situation where the energy window for the bond-center case is smaller than for the head-on case, since it has a higher E_{min} and a lower E_{max}. Therefore it is more difficult to implant an ion in the bond-center impact point than in the head-on impact point.

In the bond-center case (Table 3.14), Al, Si and P have the largest energy window due

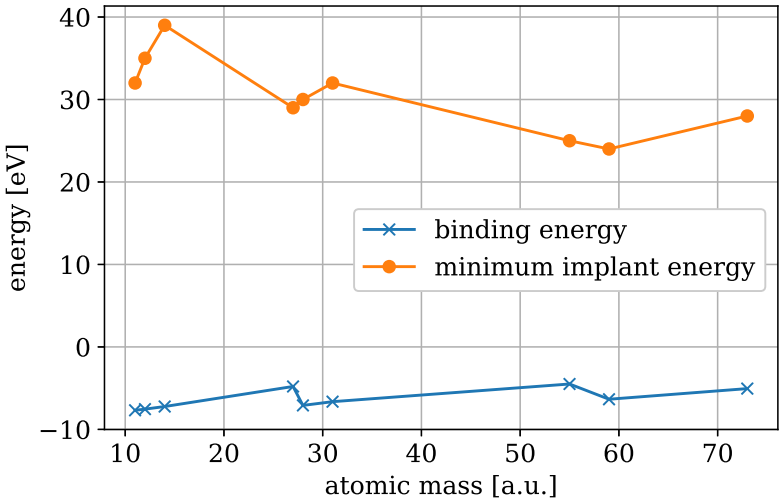

Figure 3.15: Binding energies in a divacancy, and minimum implantation energies for an impact in the center of the bond between two C atoms of B, C, N, Al, Si, P, Mn, Ni and Ge. The continuous lines were added as a guide for the eye.

to their large E_{max}. Again, C has a larger energy window than B and N, and Si has a larger energy window than Al and P.

It is interesting that, when implanting in a monovacancy, the minimum implant energy is strongly correlated with the binding energy, especially for lighter ions (Figure 3.13), but when implanting in a divacancy, the minimum energy is much less correlated with the binding energy in a divacancy (Figure 3.15).

3.3.3 Hexagon-Center Impact Point

In the case where the ion hits in the center of a graphene hexagon (Figure 1.1c), no C atom is ejected, and no implantation of the ion into the lattice was observed. E_{trans} in Table 3.15 is thus the transmission threshold energy, that is, the minimum initial energy that is needed for the ion to be transmitted through graphene. A Si ion is shown in the process of transmitting through the lattice in Figure 3.16. For Mn for an initial energy of 21 eV, the Mn ion goes through the graphene, but isn't sputtered, instead becoming an adatom on the other side of the lattice. This was not counted as the ion being transmitted through the lattice, as the ion does not really leave the lattice.

In the hexagon-center case (Table 3.15), the transmission threshold energy E_{trans} tends to be higher for heavier elements. The only exceptions are Mn and Ni, the only sub-group elements that were examined. They are found to have a lower E_{trans}.

Table 3.15: The minimum initial kinetic energy E_{trans} [eV] of the ion that results in transmission through the graphene lattice in the case where the ion hits exactly the center of a graphene hexagon.

ion	E_{trans}[eV]
B	9
C	15
N	19
Al	27
Si	29
P	35
Mn	22
Ni	23
Ge	47

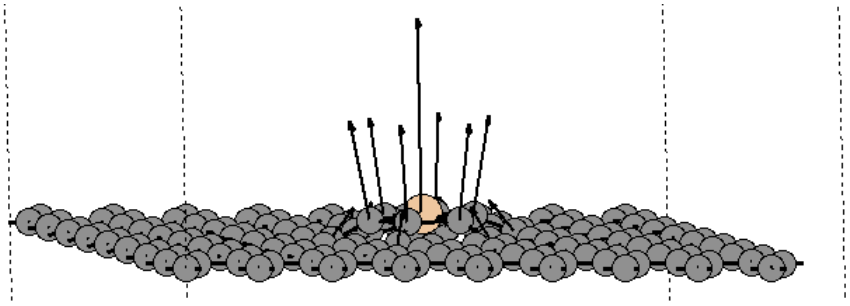

Figure 3.16: Si atom being transmitted through the center of a graphene hexagon with an initial energy of 31 eV. This image shows the system after 57 fs. The arrows indicate velocities.

3.3.4 Asymmetric Impact Point

For the asymmetrical impact point (Figure 1.1d) shown in Table 3.16, implantation occurs for only three of the ions, namely for Al, Si and P ions. For these three, there are initial energies that lead to the ions sputtering a C atom and implanting in the lattice. An example of this is show in Figure 3.17a, where an Si atom is shown being implanted. If the ion is implanted after hitting the graphene in the asymmetric impact point, the end results looks the same as the head-on outcomes in Figure 3.2, because the ion also ejects exactly one C atom.

On the other hand B, C, N, Mn, Ni and Ge ions did not implant into the lattice for any energy that was tried. There are cases where the ion is transmitted through the lattice like in the hexagon-center case (an example of this is shown with Ni in Figure 3.17b, where Ni can be seen just before escaping the lattice), but more often, it knocks out a C atom when it is transmitted. Regardless of whether or not a C atom was knocked out, when there was no energy for which implantation took place, the transmission threshold energy E_{trans} is given instead of E_{min} and E_{max}.

Table 3.16: Minimum and maximum initial kinetic energy [eV] of the ion that results in implantation in the case where the ion hits between the center of the hexagon and a C atom. In this case, for some elements, ion implantation could not be observed for any energy. For these elements, the transmission threshold energy E_{trans} is shown.

ion	E_{min}[eV]	E_{max}[eV]	E_{trans}[eV]
B	-	-	30
C	-	-	36
N	-	-	30
Al	36	46	-
Si	32	49	-
P	29	54	-
Mn	-	-	36
Ni	-	-	36
Ge	-	-	38

In the asymmetric case (Table 3.16), only Al, Si and P could be implanted in the lattice, and surprisingly, P has the largest energy window. The rest of the elements transmit through the lattice at similar values of E_{trans}.

In general, the energy window that allows implantation is widest in the head-on case, followed by the bond-center case, and then for some elements by the asymmetric case. Most tested elements do not implant at all in the asymmetric case, and none do in the hexagon-center case. A wider energy window means that implantation is more easily achieved.

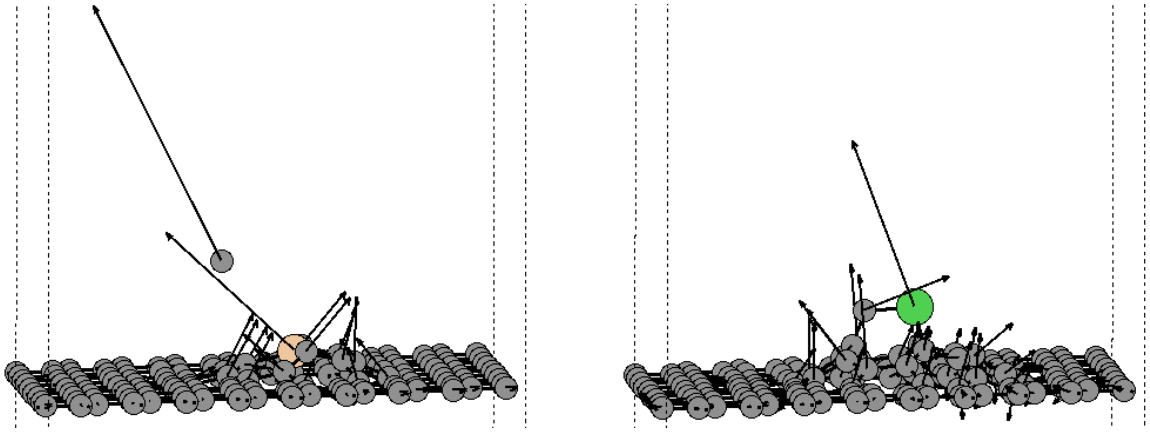

(a) Si after 71 fs.

(b) Ni after 103 fs.

Figure 3.17: Ions being fired at the asymmetric impact point with an initial energy of 40 eV. The arrows indicate velocities.

4 Conclusions

Density functional theory molecular dynamics calculations were performed to systematically study ion implantation into graphene. Four impact points were considered and minimum and maximum implantation energies were found for nine ions, namely B, C, N, Al, Si, P, Mn, Ni and Ge. For energies lower than the minimum implantation energy, the ion does not eject a C atom from the lattice, while for energies higher than the maximum implantation energy, the ion goes through the lattice. It is found that the widest range of energies that lead to implantation corresponds to the case of a head-on collision of an ion with a C atom of graphene. On the other hand, for an impact in the middle of a graphene hexagon, no implantation was observed for any energy. For an impact between these two points, some ions show a behaviour similar to the head-on case, and others similar to the hexagon-center case, meaning no implantation was observed for the latter ions. For an impact in the center of a C-C bond, the ion can eject two C atoms from the graphene and implant in the divacancy.

The obtained results suggest that the most common geometry of the implanted heteroatom will be the one where it substitutes only one C atom. In general, the energy window for implantation narrows down with the increase of the ion's mass. This happens due to the fact that the proportion of the kinetic energy transferred to a C atom becomes smaller for heavier ions. Interestingly, it was found that there is a correlation between the minimum implantation energies and the binding energies of the corresponding heteroatoms in graphene.

The cases of a heteroatom replacing two C atoms were examined further, finding that in the relaxed structures, the four C atoms neighbouring the heteroatoms tend to exhibit one of two possible geometries if the structure isn't flat: either all four neighbouring C atoms and the impurity ion protrude from the lattice, creating a pyramidal-like structure, or the C neighbours alternatingly go above and below the impurity ion, creating a tetrahedal-like geometry.

In the future, these findings could be expanded to statistically analyse which energy to use when using ion irradiation to dope graphene. DFT is too computationally expensive for this endeavour, which is why machine learning is a more promising avenue of future research. The trajectories that were obtained for this thesis can be used in the training of a machine learning algorithm, which can then be used to predict the trajectories for different impact parameters much more cheaply.

Bibliography

[1] K. S. Novoselov, A. K. Geim, S. V. Morozov, D. Jiang, Y. Zhang, S. V. Dubonos, I. V. Grigorieva, and A. A. Firsov, "Electric field effect in atomically thin carbon films," *Science*, vol. 306, no. 5696, pp. 666–669, 2004.

[2] K. I. Bolotin, K. J. Sikes, Z. Jiang, M. Klima, G. Fudenberg, J. Hone, P. Kim, and H. Stormer, "Ultrahigh electron mobility in suspended graphene," *Solid State Communications*, vol. 146, no. 9-10, pp. 351–355, 2008.

[3] A. A. Balandin, S. Ghosh, W. Bao, I. Calizo, D. Teweldebrhan, F. Miao, and C. N. Lau, "Superior thermal conductivity of single-layer graphene," *Nano letters*, vol. 8, no. 3, pp. 902–907, 2008.

[4] C. Lee, X. Wei, J. W. Kysar, and J. Hone, "Measurement of the elastic properties and intrinsic strength of monolayer graphene," *Science*, vol. 321, no. 5887, pp. 385–388, 2008.

[5] K. Kim, J.-Y. Choi, T. Kim, S.-H. Cho, and H.-J. Chung, "A role for graphene in silicon-based semiconductor devices," *Nature*, vol. 479, no. 7373, p. 338, 2011.

[6] K. Cao, S. Feng, Y. Han, L. Gao, T. H. Ly, Z. Xu, and Y. Lu, "Elastic straining of free-standing monolayer graphene," *Nature communications*, vol. 11, no. 1, pp. 1–7, 2020.

[7] Y. Touloukian, R. Powell, C. Ho, and P. Klemens, "Thermal conductivity: Nonmetallic solids, ifi," 1970.

[8] W. Bao, F. Miao, Z. Chen, H. Zhang, W. Jang, C. Dames, and C. N. Lau, "Controlled ripple texturing of suspended graphene and ultrathin graphite membranes," *Nature nanotechnology*, vol. 4, no. 9, pp. 562–566, 2009.

[9] H. Liu, Y. Liu, and D. Zhu, "Chemical doping of graphene," *Journal of materials chemistry*, vol. 21, no. 10, pp. 3335–3345, 2011.

[10] W. Li and J. Xue, "Ion implantation of low energy si into graphene: Insight from computational studies," *RSC Advances*, vol. 5, no. 121, pp. 99920–99926, 2015.

[11] G. F. Schneider, S. W. Kowalczyk, V. E. Calado, G. Pandraud, H. W. Zandbergen, L. M. Vandersypen, and C. Dekker, "DNA translocation through graphene nanopores," *Nano letters*, vol. 10, no. 8, pp. 3163–3167, 2010.

[12] Z. Yin, S. Sun, T. Salim, S. Wu, X. Huang, Q. He, Y. M. Lam, and H. Zhang, "Organic photovoltaic devices using highly flexible reduced graphene oxide films as transparent

electrodes," *ACS nano*, vol. 4, no. 9, pp. 5263–5268, 2010.

[13] F. Schedin, A. Geim, S. Morozov, E. Hill, P. Blake, M. Katsnelson, and K. Novoselov, "Detection of individual gas molecules adsorbed on graphene," *Nature materials*, vol. 6, no. 9, p. 652, 2007.

[14] A. C. Neto, F. Guinea, N. M. Peres, K. S. Novoselov, and A. K. Geim, "The electronic properties of graphene," *Reviews of modern physics*, vol. 81, no. 1, p. 109, 2009.

[15] M. Y. Han, B. Özyilmaz, Y. Zhang, and P. Kim, "Energy band-gap engineering of graphene nanoribbons," *Physical review letters*, vol. 98, no. 20, p. 206805, 2007.

[16] K. S. Novoselov, V. Fal, L. Colombo, P. Gellert, M. Schwab, K. Kim, *et al.*, "A roadmap for graphene," *Nature*, vol. 490, no. 7419, pp. 192–200, 2012.

[17] T. Ohta, A. Bostwick, T. Seyller, K. Horn, and E. Rotenberg, "Controlling the electronic structure of bilayer graphene," *Science*, vol. 313, no. 5789, pp. 951–954, 2006.

[18] T. Wehling, M. Katsnelson, and A. Lichtenstein, "Impurities on graphene: Midgap states and migration barriers," *Physical Review B*, vol. 80, no. 8, p. 085428, 2009.

[19] U. Bangert, W. Pierce, D. Kepaptsoglou, Q. Ramasse, R. Zan, M. Gass, J. Van den Berg, C. Boothroyd, J. Amani, and H. Hofsass, "Ion implantation of graphene - toward ic compatible technologies," *Nano Letters*, vol. 13, no. 10, pp. 4902–4907, 2013.

[20] D. J. Appelhans, Z. Lin, and M. T. Lusk, "Two-dimensional carbon semiconductor: Density functional theory calculations," *Phys. Rev. B*, vol. 82, no. 7, p. 073410, 2010.

[21] X.-K. Kong, C.-L. Chen, and Q.-W. Chen, "Doped graphene for metal-free catalysis," *Chemical Society Reviews*, vol. 43, no. 8, pp. 2841–2857, 2014.

[22] X. Wang, G. Sun, P. Routh, D.-H. Kim, W. Huang, and P. Chen, "Heteroatom-doped graphene materials: syntheses, properties and applications," *Chemical Society Reviews*, vol. 43, no. 20, pp. 7067–7098, 2014.

[23] J. Williams, "Ion implantation of semiconductors," *Materials Science and Engineering: A*, vol. 253, no. 1-2, pp. 8–15, 1998.

[24] E. H. Åhlgren, J. Kotakoski, and A. V. Krasheninnikov, "Atomistic simulations of the implantation of low-energy boron and nitrogen ions into graphene," *Phys. Rev. B*, vol. 83, p. 115424, Mar 2011.

[25] T. Susi, T. P. Hardcastle, H. Hofsäss, A. Mittelberger, T. J. Pennycook, C. Mangler, R. Drummond-Brydson, A. J. Scott, J. C. Meyer, and J. Kotakoski, "Single-atom spectroscopy of phosphorus dopants implanted into graphene," *2D Materials*, vol. 4, no. 2, p. 021013, 2017.

[26] M. Tripathi, A. Markevich, R. Böttger, S. Facsko, E. Besley, J. Kotakoski, and T. Susi, "Implanting germanium into graphene," *ACS Nano*, vol. 12, no. 5, pp. 4641–4647, 2018. PMID: 29727567.

[27] L. Zhao, R. He, K. T. Rim, T. Schiros, K. S. Kim, H. Zhou, C. Gutiérrez, S. Chock-

alingam, C. J. Arguello, L. Pálová, *et al.*, "Visualizing individual nitrogen dopants in monolayer graphene," *Science*, vol. 333, no. 6045, pp. 999–1003, 2011.

[28] L. Zhao, M. Levendorf, S. Goncher, T. Schiros, L. Palova, A. Zabet-Khosousi, K. T. Rim, C. Gutierrez, D. Nordlund, C. Jaye, *et al.*, "Local atomic and electronic structure of boron chemical doping in monolayer graphene," *Nano letters*, vol. 13, no. 10, pp. 4659–4665, 2013.

[29] W. Zhou, M. D. Kapetanakis, M. P. Prange, S. T. Pantelides, S. J. Pennycook, and J.-C. Idrobo, "Direct determination of the chemical bonding of individual impurities in graphene," *Physical review letters*, vol. 109, no. 20, p. 206803, 2012.

[30] Q. M. Ramasse, C. R. Seabourne, D.-M. Kepaptsoglou, R. Zan, U. Bangert, and A. J. Scott, "Probing the bonding and electronic structure of single atom dopants in graphene with electron energy loss spectroscopy," *Nano letters*, vol. 13, no. 10, pp. 4989–4995, 2013.

[31] A. V. Krasheninnikov, Y. Miyamoto, and D. Tománek, "Role of electronic excitations in ion collisions with carbon nanostructures," *Physical review letters*, vol. 99, no. 1, p. 016104, 2007.

[32] E. Gruber, R. A. Wilhelm, R. Pétuya, V. Smejkal, R. Kozubek, A. Hierzenberger, B. C. Bayer, I. Aldazabal, A. K. Kazansky, F. Libisch, *et al.*, "Ultrafast electronic response of graphene to a strong and localized electric field," *Nature communications*, vol. 7, no. 1, pp. 1–7, 2016.

[33] A. Krasheninnikov, P. Lehtinen, A. S. Foster, P. Pyykkö, and R. M. Nieminen, "Embedding transition-metal atoms in graphene: structure, bonding, and magnetism," *Physical review letters*, vol. 102, no. 12, p. 126807, 2009.

[34] E. J. Santos, A. Ayuela, and D. Sánchez-Portal, "First-principles study of substitutional metal impurities in graphene: structural, electronic and magnetic properties," *New Journal of Physics*, vol. 12, no. 5, p. 053012, 2010.

[35] M. Kaukonen, A. Krasheninnikov, E. Kauppinen, and R. Nieminen, "Doped graphene as a material for oxygen reduction reaction in hydrogen fuel cells: a computational study," *ACS catalysis*, vol. 3, no. 2, pp. 159–165, 2013.

[36] M. Orio, D. A. Pantazis, and F. Neese, "Density functional theory," *Photosynthesis research*, vol. 102, no. 2-3, pp. 443–453, 2009.

[37] A. Krasheninnikov and K. Nordlund, "Ion and electron irradiation-induced effects in nanostructured materials," *Journal of applied physics*, vol. 107, no. 7, p. 3, 2010.

[38] P. Hohenberg and W. Kohn, "Inhomogeneous electron gas," *Phys. Rev.*, vol. 136, pp. B864–B871, Nov 1964.

[39] D. Sholl and J. A. Steckel, *Density functional theory: a practical introduction*. John Wiley & Sons, 2011.

[40] W. Koch and M. C. Holthausen, *A chemist's guide to density functional theory*. John

Wiley & Sons, 2015.

[41] J. P. Perdew, K. Burke, and M. Ernzerhof, "Generalized gradient approximation made simple," *Physical review letters*, vol. 77, no. 18, p. 3865, 1996.

[42] "Gpaw: Dft and beyond within the projector-augmented wave method." https://wiki.fysik.dtu.dk/gpaw/. Accessed: 2020-04-15.

[43] L. Pauling, "The application of the quantum mechanics to the structure of the hydrogen molecule and hydrogen molecule-ion and to related problems.," *Chemical Reviews*, vol. 5, no. 2, pp. 173–213, 1928.

[44] P. E. Blöchl, C. J. Först, and J. Schimpl, "Projector augmented wave method: ab initio molecular dynamics with full wave functions," *Bulletin of Materials Science*, vol. 26, no. 1, pp. 33–41, 2003.

[45] H. Hellmann, "A new approximation method in the problem of many electrons," *The Journal of Chemical Physics*, vol. 3, no. 1, pp. 61–61, 1935.

[46] P. Schwerdtfeger, "The pseudopotential approximation in electronic structure theory," *ChemPhysChem*, vol. 12, no. 17, pp. 3143–3155, 2011.

[47] D. Vanderbilt, "Soft self-consistent pseudopotentials in a generalized eigenvalue formalism," *Physical review B*, vol. 41, no. 11, p. 7892, 1990.

[48] J. C. Slater, "Wave functions in a periodic potential," *Phys. Rev.*, vol. 51, pp. 846–851, May 1937.

[49] P. F. Baumeister and S. Tsukamoto, "Analytical paw projector functions for reduced bandwidth requirements," in *Proceedings of the Platform for Advanced Scientific Computing Conference*, pp. 1–11, 2019.

[50] J. J. Mortensen, L. B. Hansen, and K. W. Jacobsen, "Real-space grid implementation of the projector augmented wave method," *Phys. Rev. B*, vol. 71, p. 035109, JAN 2005.

[51] A. H. Larsen, M. Vanin, J. J. Mortensen, K. S. Thygesen, and K. W. Jacobsen, "Localized atomic basis set in the projector augmented wave method," *Phys. Rev. B*, vol. 80, p. 195112, Nov 2009.

[52] A. H. Larsen, J. J. Mortensen, J. Blomqvist, I. E. Castelli, R. Christensen, M. Dułak, J. Friis, M. N. Groves, B. Hammer, C. Hargus, E. D. Hermes, P. C. Jennings, P. B. Jensen, J. Kermode, J. R. Kitchin, E. L. Kolsbjerg, J. Kubal, K. Kaasbjerg, S. Lysgaard, J. B. Maronsson, T. Maxson, T. Olsen, L. Pastewka, A. Peterson, C. Rostgaard, J. Schiøtz, O. Schütt, M. Strange, K. S. Thygesen, T. Vegge, L. Vilhelmsen, M. Walter, Z. Zeng, and K. W. Jacobsen, "The atomic simulation environment—a python library for working with atoms," *Journal of Physics: Condensed Matter*, vol. 29, no. 27, p. 273002, 2017.

[53] "Atomic simulation environment." https://wiki.fysik.dtu.dk/ase/index.html. Accessed: 2020-04-15.

[54] H. J. Monkhorst and J. D. Pack, "Special points for brillouin-zone integrations," *Physical review B*, vol. 13, no. 12, p. 5188, 1976.

[55] G. Chiarotti, "1.6 crystal structures and bulk lattice parameters of materials quoted in the volume," in *Interaction of Charged Particles and Atoms with Surfaces*, pp. 21–26, Springer, 1995.

[56] "Nist computational chemistry comparison and benchmark database." NIST Standard Reference Database Number 101. Release 21, August 2020, Editor: Russell D. Johnson III http://cccbdb.nist.gov/.

[57] B. Ruscic, D. Feller, and K. A. Peterson, "Active thermochemical tables: dissociation energies of several homonuclear first-row diatomics and related thermochemical values," in *Thom H. Dunning, Jr.*, pp. 191–202, Springer, 2015.

[58] I. A. Pašti, A. Jovanović, A. S. Dobrota, S. V. Mentus, B. Johansson, and N. V. Skorodumova, "Atomic adsorption on graphene with a single vacancy: systematic dft study through the periodic table of elements," *Physical Chemistry Chemical Physics*, vol. 20, no. 2, pp. 858–865, 2018.

[59] "Van der waals radius of the elements." https://periodictable.com/Properties/A/VanDerWaalsRadius.an.html. Accessed: 2020-07-07.

[60] M. Mantina, A. C. Chamberlin, R. Valero, C. J. Cramer, and D. G. Truhlar, "Consistent van der waals radii for the whole main group," *The Journal of Physical Chemistry A*, vol. 113, no. 19, pp. 5806–5812, 2009.

[61] "Webelements." https://www.webelements.com. Accessed: 2020-11-10.

[62] T. Susi, C. Hofer, G. Argentero, G. T. Leuthner, T. J. Pennycook, C. Mangler, J. C. Meyer, and J. Kotakoski, "Isotope analysis in the transmission electron microscope," *Nature communications*, vol. 7, no. 1, pp. 1–10, 2016.

5 Supplement

k-point convergence in PW-mode

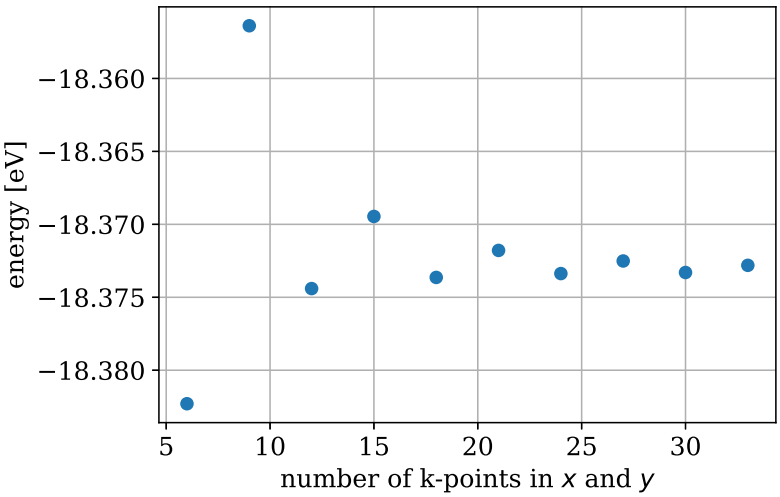

Figure 5.1: Number of k-points and the corresponding energy of the system for PW-mode with a cutoff energy of 450 eV.

PW cutoff energy convergence

In PW-mode, the energies for different cutoff energies were calculated.
$k = (24 \times 24 \times 1)$, $a = 2.4678$, $c = 20.0$. (Figure 5.2)

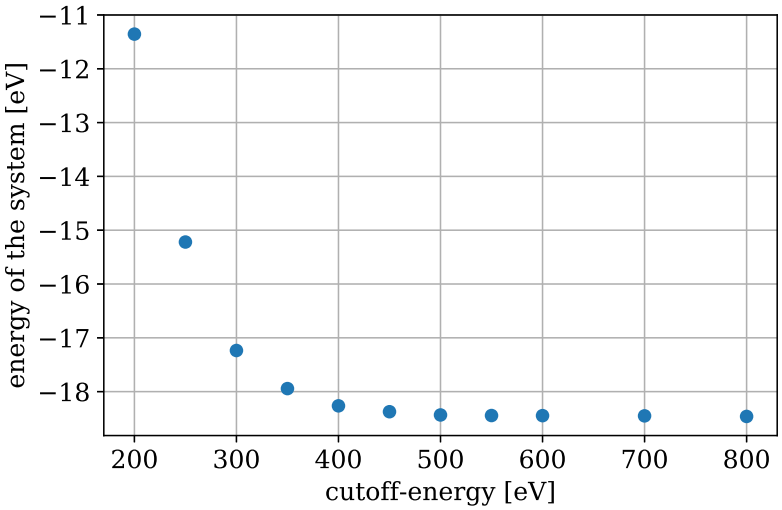

Figure 5.2: The energy of the system for different cutoff energies in PW mode.

Varying the Space-step ds

So far, to check what the largest possible timestep is that still yields results with reasonable computational accuracy, the same simulation was done multiple times using different timesteps and comparing the results. However, this does not take into account that a smaller timestep is needed if the atoms are moving faster, as they then cover a greater distance during a given time. Above, the simulations were done for 22 eV and 100 eV, and it was shown that a smaller timestep is needed to reach energy conservation for the higher initial ion energy.

For the purposes of this thesis, the distance that is covered during one timestep will be called a space-step ds. Here, a different approach analogous to that in Section 2.4.1 is be tried: Using the same cell as before, and gpts = $(56 \times 56 \times 56)$, the initial space-step ds_0 and the initial energy E_{in} were varied. The timestep dt was calculated from the initial energy and the initial space-step ds_0 as follows:

$$dt = \frac{ds_0}{v_0} = \frac{ds_0}{\sqrt{\frac{2 \cdot E_{in}}{m}}} \tag{5.1}$$

where v_0 is the initial velocity of the ion and m is the mass of the ion. Thus, if a low value is chosen for ds_0 this results in a small timestep dt and high computational time. As the velocity of the ion v changes in the course of the simulation, the space-step ds changes too. However, the timestep dt is only calculated at the very beginning from the initial energy v_0, thus dt remains constant during the whole simulation. The units of the space-step ds are

$$1ds = 1 \text{ fs}\sqrt{\text{eV/u}} \approx 0.0982 \text{ Å} \tag{5.2}$$

As shown in the following figures, the computational accuracy still depends on E_{in}. The reason for this is that the velocity of the atoms changes during the calculation. Presumably, if dt were re-calculated at every timestep so that ds stays constant, then the results of the calculations should not depend on E_{in}.

Figure 5.3c and d show that lower energy is the least-well conserved especially for high ds_0. This is probably due to the fact that for a low initial velocity a small change in absolute velocity means a large change in relative velocity. However, interestingly, lower energy also results in *more* collisions in a row than higher energy, but only if a low value is chosen for ds_0.

For $E_{in} = 1000$ eV, an error occurs, even for $ds_0 = 3$ where $dt = 0.23$ fs, which is not an unreasonably small timestep.

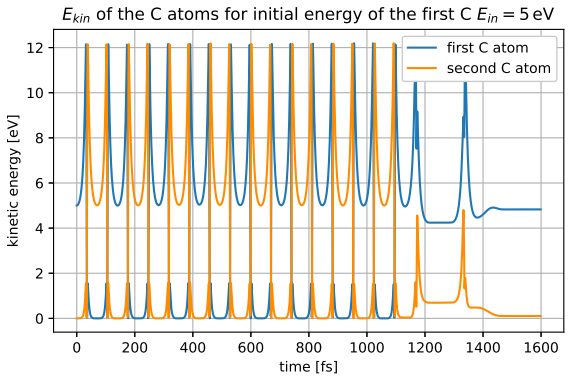

(a) $ds_0 = 0.5$, therefore $dt \approx 0.55$ fs.

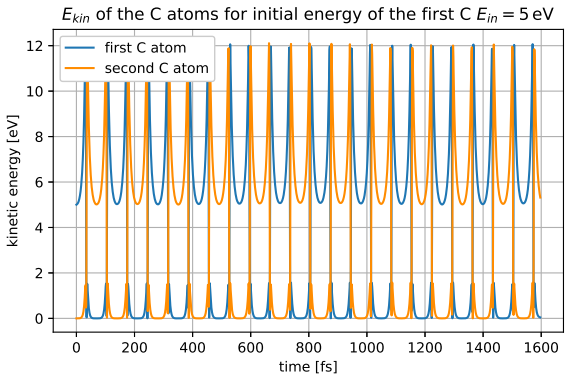

(b) $ds_0 = 1.0$, therefore $dt \approx 1.1$ fs.

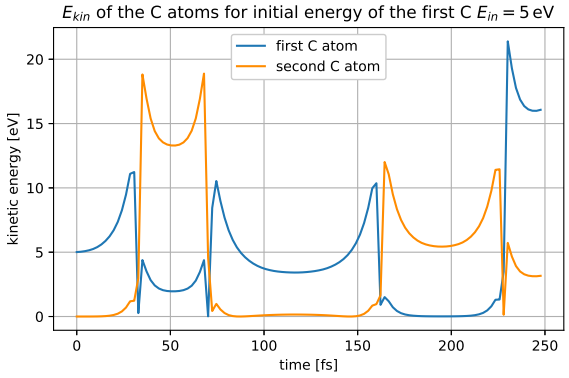

(c) $ds_0 = 2.0$, therefore $dt \approx 2.2$ fs.

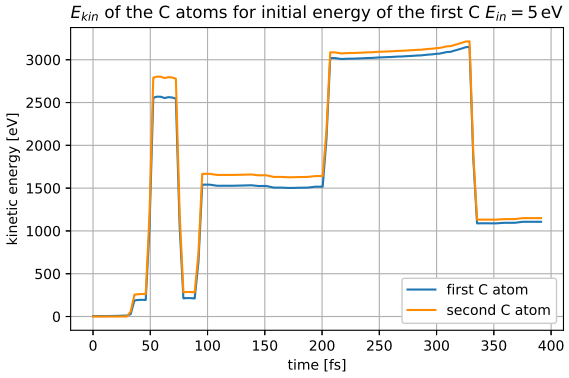

(d) $ds_0 = 3.0$, therefore $dt \approx 3.3$ fs.

Figure 5.3: Kinetic energy of the two C atoms for $E_{in} = 5$ eV.

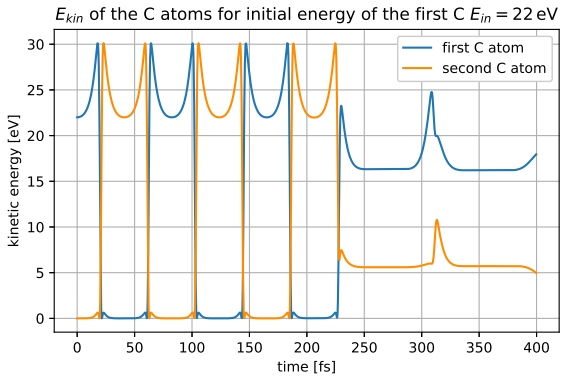

(a) $ds_0 = 0.5$, therefore $dt \approx 0.26$ fs.

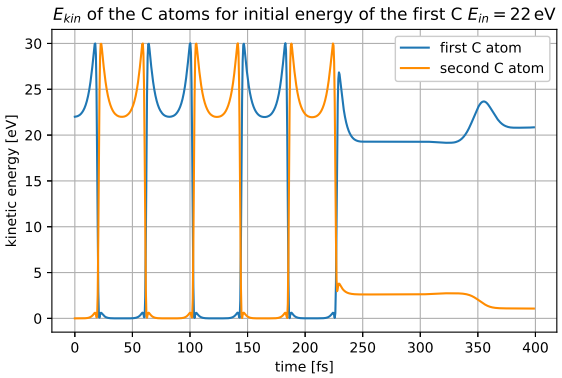

(b) $ds_0 = 1.0$, therefore $dt \approx 0.52$ fs.

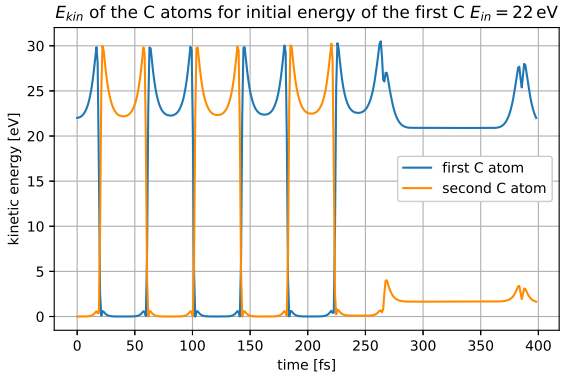

(c) $ds_0 = 2.0$, therefore $dt \approx 1.0$ fs.

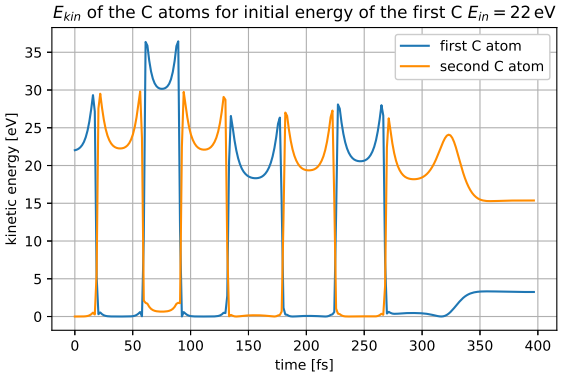

(d) $ds_0 = 3.0$, therefore $dt \approx 1.6$ fs.

Figure 5.4: Kinetic energy of the two C atoms for $E_{in} = 22$ eV.

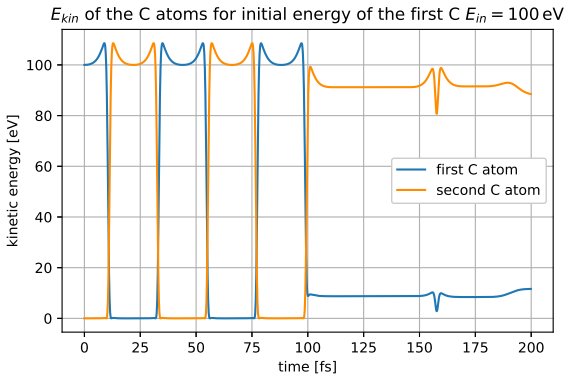

(a) $ds_0 = 0.5$, therefore $dt \approx 0.12$ fs.

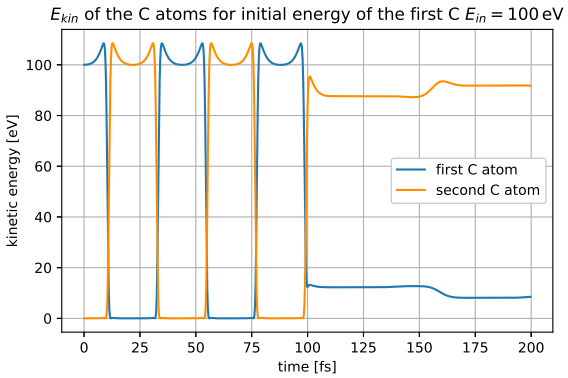

(b) $ds_0 = 1.0$, therefore $dt \approx 0.25$ fs.

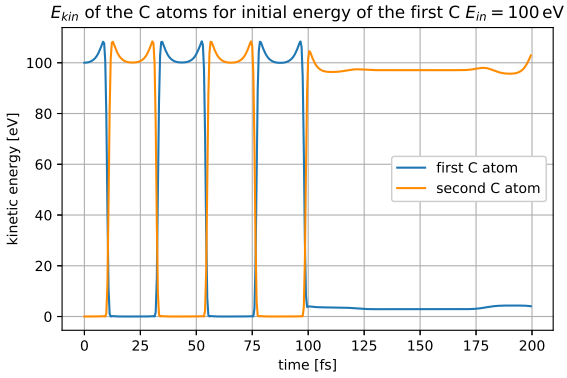

(c) $ds_0 = 2.0$, therefore $dt \approx 0.49$ fs.

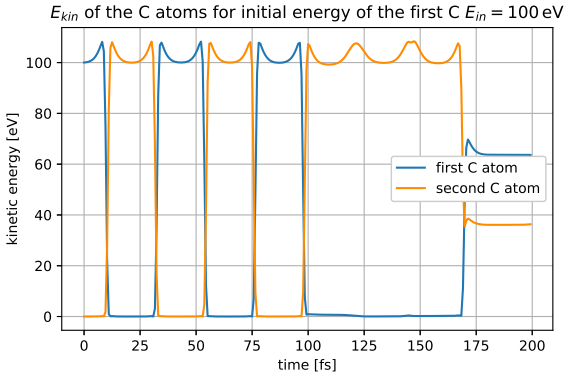

(d) $ds_0 = 3.0$, therefore $dt \approx 0.74$ fs.

Figure 5.5: Kinetic energy of the two C atoms for $E_{in} = 100$ eV.

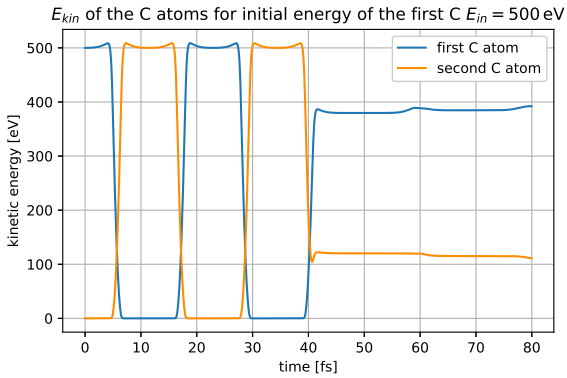

(a) $ds_0 = 0.5$, therefore $dt \approx 0.05$ fs.

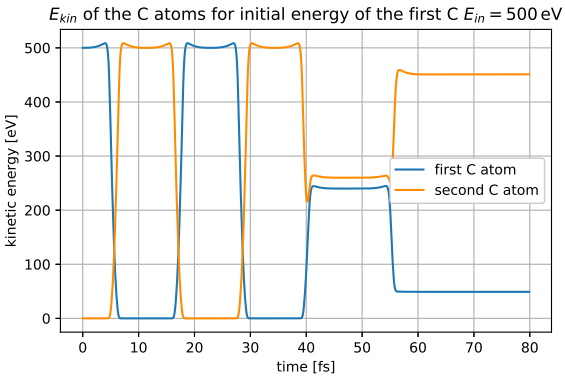

(b) $ds_0 = 1.0$, therefore $dt \approx 0.11$ fs.

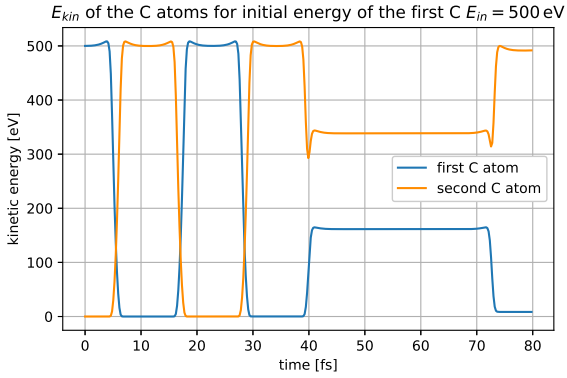

(c) $ds_0 = 2.0$, therefore $dt \approx 0.22$ fs.

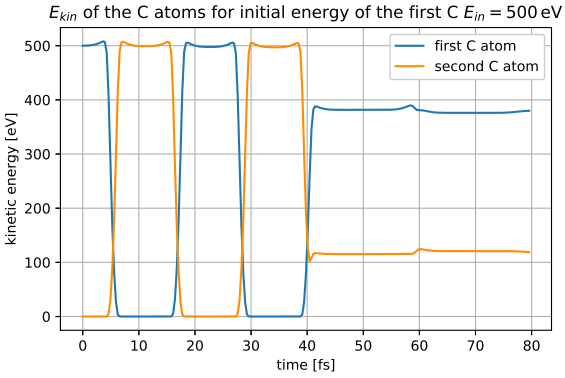

(d) $ds_0 = 3.0$, therefore $dt \approx 0.33$ fs.

Figure 5.6: Kinetic energy of the two C atoms for $E_{in} = 500$ eV.